1H-NMR METABOLOMICS CHARACTERIZES TRANSITION FROM EBB TO FLOW IN A PORCINE MODEL OF SMOKE INHALATION AND SEVERE BURN INJURY

A THESIS SUBMITTED TO THE FACULTY OF THE GRADUATE SCHOOL OF THE UNIVERSITY OF MINNESOTA BY

Cole Grant Hendrickson

IN PARTIAL FULFILLMENT OF THE REQUIREMENTS FOR THE DEGREE OF MASTER OF SCIENCE

June 2018

© 2018 Cole Grant Hendrickson

ACKNOWLEDGEMENTS

I would like to thank my committee members Dr. Gregory Beilman, Dr. Elizabeth Lusczek, Dr. Peter Crawford, and Dr. Lester Drewes for their support in the completion of this master's thesis. Dr. Luszcek in particular provided excellent mentorship on the fundamentals of NMR metabolomics, and Dr. Beilman on the overarching principles of clinical burn physiology. I would also like to thank my fellow lab members Kristine Mueller, Mariya Skube, Andrea Wolf, and Mark Stice for their feedback and encouragement. This work could not have been completed without the help and services of the Minnesota NMR Center or the previous work done by our collaborators at the US Army Institute of Surgical Research in Houston, Texas. Special thanks must be given to the Institute of Surgical Research for performing the animal portion of this study and for providing serum samples and blood gas data for our analysis. Finally, I would like to thank the members of my cohort in the Integrated Biosciences Department at the University of Minnesota Duluth and my family and friends for sticking with me during this phase of my education and career development.

ABSTRACT

Burn injury initiates a metabolic response that, even when treated, causes muscle wasting and organ dysfunction in burn patients as long as two years following injury. This increased metabolic rate, termed “flow” phase in burn physiology, is initially masked by low blood pressure and inadequate oxygen supply in burn shock, known as “ebb” phase. Our study examined the metabolic transition between the “ebb” and “flow” phases of burn recovery using proton nuclear magnetic resonance (^{1}H-NMR) spectroscopy in a porcine model of severe burn injury with additional smoke inhalation. We hypothesized the serum metabolomes of porcine subjects would be distinguishable by time point, and the changes in individual metabolite concentrations would characterize the shift from “ebb” to “flow” in burn physiology. Fifteen pigs received 40% total body surface area (TBSA) thermal burns with additional pine bark smoke inhalation treatment. Subjects were resuscitated and kept anesthetized until 72 hours post-burn or death. Arterial blood samples were drawn at baseline (pre-burn) and every 24 hours until 72 hours post-injury or death. The aqueous portion of each sample was analyzed in a 700MHz spectrometer and metabolite peaks were fit to spectra using Chenomx software. Thirty-eight metabolites were detected in 39 samples, and principal component analysis (PCA) was conducted to separate samples by time point. 51.6% of metabolite variability was captured in the first two principal components. We found post-burn metabolomes of porcine subjects to be distinguishable by time point using ^{1}H-NMR and principal component analysis. We also constructed a framework for non-lactic acidosis in resuscitated burn subjects that emphasized oxidative stress and increased fatty acid

catabolism as root causes of organic acid accumulation. Further studies will be required to confirm and elaborate on the post-burn metabolic pathways suggested by this analysis.

TABLE OF CONTENTS

List of Tables

List of Figures

CHAPTER 1

INTRODUCTION

Overview of Burn Injury

Burn injury is characterized by tissue damage resulting from exposure to heat, cold, radiation, reactive chemicals, or electricity. A full-thickness burn is a burn in which both layers of the skin, the dermis and the epidermis, are destroyed by contact with the heat source. Injury severity is often quantified by estimating the total body surface area (TBSA) that is covered by full-thickness burn. Without proper treatment, burns as small as 20% TBSA can be fatal. An estimated 140,000 deaths are attributed to burn injury each year (1), and over 3000 of those deaths occur in the United States, where the highest level of burn treatment is available (2).

"Ebb" and "Flow" in Burn Metabolism

The metabolic response to burn injury was first described in 1942 by D.P. Cuthbertson, who divided recovery from critical injury into an "ebb" phase and a "flow" phase (3). Since that time, "ebb" and "flow" has become a central paradigm in the study of burn physiology (Figure 1). "Flow" dynamics dominate long-term burn recovery, where increased metabolic rates depend on tissue catabolism that can compromise organ function and immune response in severely burned patients. Hypermetabolism is initially blunted, however, by hypovolemic shock that characterizes the "ebb" phase of recovery. Low blood pressure and inadequate oxygen delivery immediately following injury make it impossible for the body to mount a hypermetabolic response, so only after the patient

has been resuscitated from the shock state can the transition from hypodynamic to hyperdynamic metabolism be observed.

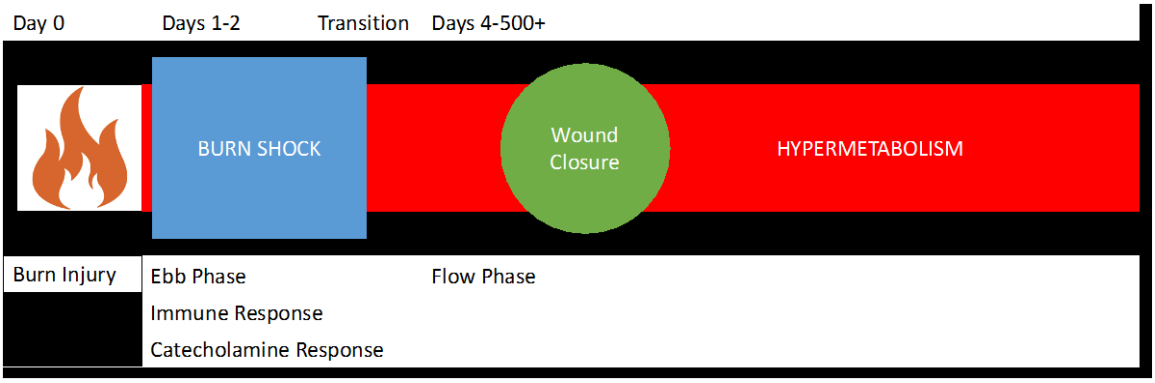

Figure 1. Burn injury initiates immediate immune and sympathetic (adrenergic) responses that control hypermetabolic dynamics long-term. However, the effects are initially covered by hypodynamic burn shock that also closely follows injury. Once shock is resolved, patients' metabolic rates can remain elevated for as long as two years post-injury.

Wound Healing in Burn Injury

Wound healing begins immediately after initial insult in burn injury. Cytokines released by damaged cells attract immune cells to the site of injury (4), and histamine released near the wound site allows macrophages and polymorphonuclear (PMN) cells to infiltrate the tissue through tight junctions in the cardiovascular epithelium (5, 6). Afferent signals to the hypothalamus cause it to stimulate catecholamine release from the adrenal glands, which increases breakdown of fat, protein, and glycogen to fuel the sympathetic response to injury. If catecholamine supplies cannot be maintained through increased tyrosine cycling, the patient will become hypothermic and their chances of survival will decrease dramatically (7).

Leukocytes and fibroblasts in the wound area maintain a preference for anaerobic glycolysis even after oxygen delivery has been restored, so glucose produced in the liver is primarily shuttled to the wound site to support wound healing activities. Glucogenic amino acids are transported from muscle to the liver primarily in the form of alanine as part of the glucose-alanine cycle (8), and glycerol from triglycerides can also be used for gluconeogenesis (Figure 2) (9). At the same time, lactic acid produced at the wound site is transported to the liver where it is packaged back into glucose for export as part of the Cori cycle. Free fatty acids, which cannot be used for gluconeogenesis, become the primary source of fuel for vital organs including the liver and peripheral tissues while wound healing continues.

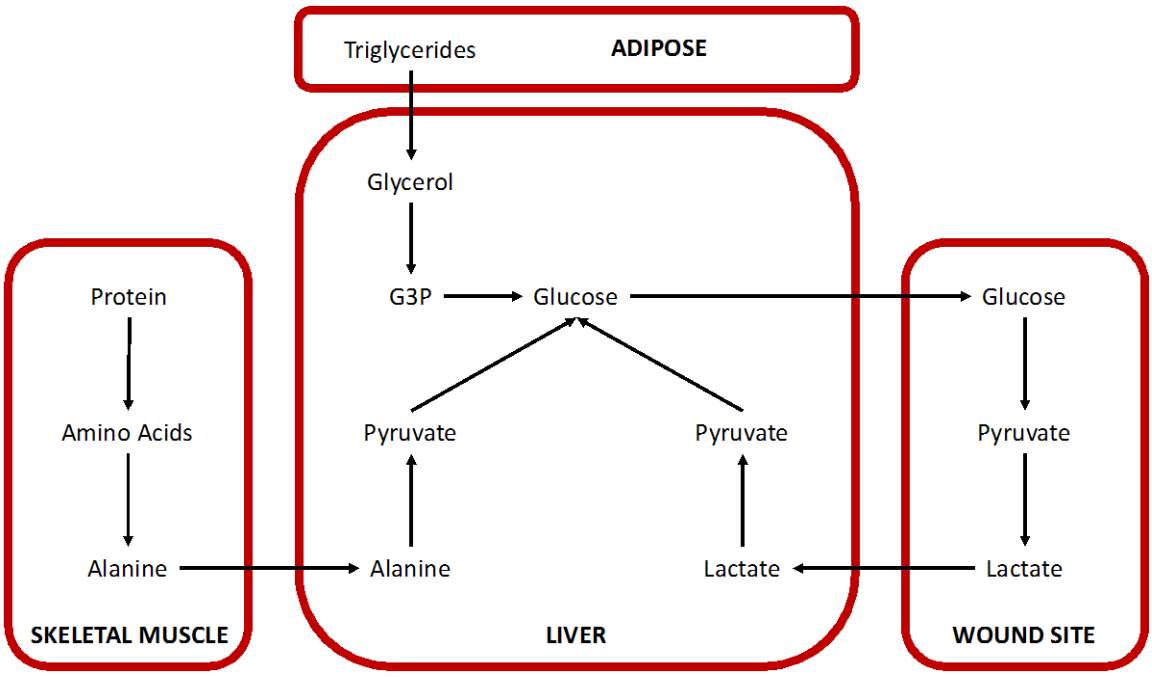

Figure 2. Gluconeogenic substrates come to the liver from adipose tissue as glycerol, from skeletal muscle as protein, and from anaerobic tissues as lactate. Glucose would normally cycle back to skeletal muscle for aerobic glycolysis, but hormonal conditions

following burn prioritize glucose for the wound site, instead breaking down muscle proteins and using fatty acids to fuel muscle function.

Common Response to Critical Injury

Evidence has shown the metabolic response to burn is the common response of the body to all mechanisms of traumatic injury. Xiao *et al.* published a seminal paper wherein they analyzed transcriptomes of human immune cells following various forms of injury (10). They observed a massive shift in gene expression during the first twelve hours of injury from the expression of genes supporting specific immunity to the expression of genes supporting innate immunity. This response was similar across all mechanisms of injury examined, and the magnitude of the shift was correlated with severity of injury and magnitude of hypermetabolism. Circulating catecholamine levels have also been correlated with injury severity and hypermetabolic response in burn injury (6), suggesting inflammation, catecholamines, and hypermetabolism are all interrelated in burn recovery.

Smoke Inhalation Injury

Fire and flame burn is the most common mechanism of burn injury, accounting for 46% of all burn cases (11). At least half of those cases present with accompanying smoke inhalation injury due to combustion of building materials or furniture (12). Though the metabolic effects of smoke inhalation injury are similar to those of external burn injury, the most dangerous effects of smoke inhalation more often relate to inhaled toxic chemicals in the lower airways than to heat injury of the upper respiratory system. Airway obstruction (edema), cyanide or carbon monoxide poisoning, and pneumonia associated with smoke inhalation can raise the risk of mortality in burn victims by as

much as 100% when compared to similarly burn patients without inhalation injury (13, 14).

Metabolomics in Medical Research

Metabolomics affords the closest approximation of an organism's molecular phenotype (Figure 3) (15). Genomics is limited by unknown rates of gene transcription of DNA to RNA. Transcriptomics is limited by unknown translational activity from RNA to protein. Proteomics is limited by unknown protein activity due to post-translational regulation. Metabolomics, however, shows the intermediate and end products of all those higher-level processes. The collected sum of metabolites in a given biological compartment shows the breakdown, synthesis, and activity of any protein produced to support cell function. Changes in metabolite concentrations can therefore indicate changes in cell function due to various disease pathologies. Metabolomics has been used previously in medical research to describe metabolic changes associated with trauma (16-19), cognitive impairment (20), sepsis (21), and even burn injury (22-24), amongst many other pathologies.

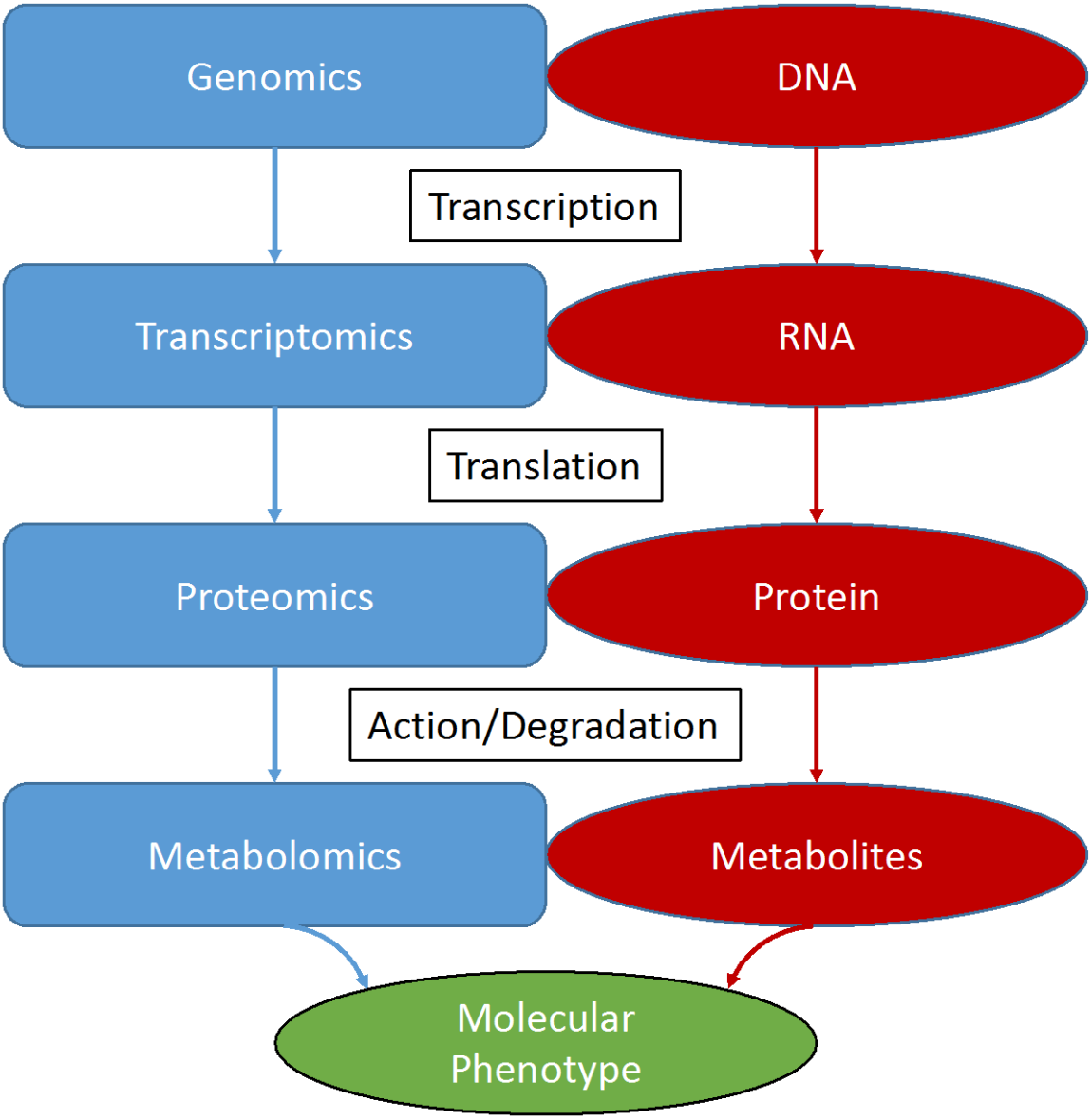

Figure 3. The phenotype of an organism is the observable set of characteristics resulting from the interaction of the organism's genome with the environment. In other words, the phenotype is the result of transcription, translation, action, and degradation of gene products as allowed by the cell or organism's energetic and molecular environment. Metabolites are the intermediates and direct products of protein action, resulting in the closest approximation of an organism's phenotype.

Objectives and Hypothesis

Our goal in this study was to examine the metabolic transition between the "ebb" and "flow" phases of burn recovery using proton nuclear magnetic resonance (^{1}H-NMR) spectroscopy in a porcine model of severe burn injury with additional smoke inhalation. We hypothesized that serum metabolomes of porcine subjects would be distinguishable by time point, and the changes in individual metabolite concentrations would characterize the shift from "ebb" to "flow" in burn physiology.

CHAPTER 2

MATERIALS AND METHODS

We performed a secondary analysis of serum samples from a study at the US Army Institute of Surgical Research (ISR) utilizing a porcine model of burn injury and smoke inhalation. Details of the study performed by the ISR, which sought to test the safety and efficacy of a particular hemoadsorption product for filtering cytokines from subjects' blood following severe burn injury with additional smoke inhalation treatment, have been previously described (25). All animal protocols herein described were approved by and performed at the US Army Institute of Surgical Research and were compliant with the Animal Welfare Act and The Guide for the Care and Use of Laboratory Animals (26, 27).

Burn and Smoke Inhalation Protocol

Female, non-pregnant, Yorkshire pigs were (n=15) were anesthetized with total intravenous anesthesia (5-15 µg/kg/hr fentanyl, 0.1-0.5 µg/kg/hr midazolam, 10-30 mg/kg/hr ketamine, 0.5-3 mg/kg/hr propofol) for the duration of the experiment. Catheters were placed in the left carotid artery and in the pulmonary artery via the left jugular vein. An additional dialysis catheter was placed in the right jugular vein for extracorporeal blood treatment. Tracheostomy was performed to administer smoke inhalation injury. Pine bark was burned in a custom chamber, designed to mix room air and oxygen, prior to cooling and administration via tracheostomy. Tidal volume per smoke breath was set at 30mL/kg body weight with a desired inhalation endpoint of 80-90% arterial carboxyhemoglobin as determined by blood gas analysis. A Bunsen burner

was used to apply full-thickness burns on each flank, 20% TBSA on each side. Animals were then transferred to the animal ICU, where they were resuscitated with lactated Ringer's volumes guided by computerized decision support software, the Burn Resuscitation Decision Support System (BRDSS) (28). BRDSS guidance was replaced by manual calculation of 0.45% sodium chloride and 5% glucose volumes following stabilization or at 48 hours post-burn. Subjects were fasted from 24 hours prior to the experiment.

Extracorporeal Treatments

Animals were randomized to extracorporeal blood treatment groups using either a CytoSorb hemoadsorption column (n=9) (CytoSorbents Corporation, Monmouth Junction, New Jersey) or a sham extracorporeal circuit (n=6) prior to the start of the experiment. Subjects underwent 6-hour extracorporeal treatment sessions starting immediately after burn and smoke inhalation treatment and recurring at 24-hour intervals thereafter. Blood was drawn at baseline (pre-burn) and every day prior to extracorporeal treatment. Animals were observed for 72 hours or until death. Serum was extracted and stored at -80°C. All animals were euthanized at the end of the study in accordance with the American Veterinary Medical Association Guidelines on Euthanasia from June, 2007 (29).

Serum Sample Processing

Serum was stored at -80°C until analysis. Samples were thawed and filtered using 3 kDa Centrifee® centrifugal filters (Merck Millipore Ltd, Darmstadt, Germany) at 4°C and

6000 rpm for 2-3 hours. A 250 μL filtrate sample was combined with 250 μL sodium phosphate buffer prepared with D_2O. Fifty microliters of the internal standard 3-(trimethylsilyl)propionic acid (TSP, Sigma-Aldrich, St. Louis, MO, USA) were added to a concentration of 0.5 mM. Final pH was recorded and the solution was transferred to 5 mm NMR tubes for immediate analysis.

Proton Nuclear Magnetic Resonance (^{1}H-NMR) Spectroscopy

^{1}H-NMR spectra were collected using a Bruker Avance spectrometer with autosampler and 5 mm triple resonance ^{1}H, ^{13}C, and ^{15}N TXI CryoProbe with Zgradient running TopSpin v. 2.16 (Bruker BioSpin, Fremont, CA, USA) at 700.13 MHz. A 1D Carr-Purcell-Meiboom-Gill (CPMG) pulse sequence was used with a relaxation time defined by the 90° pulse width calibrated for each sample. Relaxation delay was 2 s, acquisition time was 3 s, spectral width was 10 KHz, total data points collected were 63,000, and number of transients collected were 128. All spectra were collected at 298 K.

Spectral Analysis

All spectra were analyzed with an untargeted approach using Chenomx software (Edmonton, AB, Canada) (30). Manual phasing and baseline correction as well as the Chenomx Reference Deconvolution algorithm were applied to spectra before targeted profiling was performed. Identified metabolites were fit to each spectrum by the same human operator, resulting in sample profiles consisting of each metabolite and its concentration in millimoles per liter (mM).

Statistical Analysis

Statistical analysis was performed using R software (31). Principal component analysis (PCA) was used for multivariate analysis as an unsupervised method for discriminating group membership based on overall variability in metabolomic profiles. Partial least squares discriminant analysis (PLS-DA) was considered for supervised discrimination of time point groups, but we encountered a number of issues. First, a paper from Brereton suggested PLS-DA was inappropriate for discrimination of more than two output groups (32), and our analysis contains four groups. Furthermore, after examining the code of a commonly used PLS-DA platform (33, 34) that specified partial least squared regression (PLSR) analysis in its code, we were not convinced the platform was performing a discriminatory analysis rather than a regression analysis for our purposes. Finally, in the case of the DiscriMiner package, we were not convinced of its methods for combining Q^2 values from multiple one-vs-all PLS-DA models (35). No explanation was given by the authors of the DiscriMiner package for their methods of combining predicted residual error sum of squares (PRESS) and residual sum of squares (RSS) statistics from each model into a global predictive figure (Q^2).

Metabolite concentrations were log-transformed and scaled to unit variance prior to use in principal component analysis (PCA). The "FactoMineR" package (36) was used for PCA calculation and the "factoextra" package (37) was used for ggplot2-based visualization of PCA outputs. The first two principal components from PCA were projected onto an X-Y bi-plot of scores and loadings for visual interpretation. Ranked contributions of individual metabolites to overall variability in the data were calculated

using their contribution to variation in the first two principal components weighted by the eigenvalues for those principal components. Because overall variability accounts for group separation in the two-component scores plot, contribution scores also ranked the contributions made by individual metabolites to group separation in the two-component model. Group membership was determined according to hemoadsorption treatment and time point in two separate PCA models.

Kruskal-Wallis testing was used as a non-parametric univariate method to calculate significant metabolite concentration differences ($p<0.05$) between treatment groups (hemoadsorption vs. sham) and significant concentration changes ($p<0.05$) over all time points (0h, 24h, 48h, and 72h). Bonferonni multiple test correction was used to designate a subgroup of metabolites that were significant after adjustment for 38 tests ($p<0.0013$). Due to the nature of Kruskal-Wallis testing for more than two groups, a significant result indicated the concentration of that metabolite was significantly different at one or more time points compared to the others, but it did not provide further information about the relative concentrations of that metabolite over time. Correlations between blood gas variables were evaluated using Pearson correlation. The “ggplot2” package (38) was used to make box plots and scatterplots depicting individual metabolite concentration trends and blood gas correlations.

CHAPTER 3

RESULTS

Sample Collection and ^{1}H-NMR Data

The study began with 15 subjects at the baseline time point (0h), and 5 subjects survived until 72 hours (Table 1). Survival differences between treatment groups based on mean survival time in hours were not statistically significant (25). ^{1}H-NMR spectra were obtained for all 39 samples. 38 metabolite peaks were matched to each spectrum (Figure 4) using Chenomx software (Table 2).

Time point	Hemoadsorption	Sham	Total Samples
0h	9	6	15
24h	6	5	11
48h	4	4	8
72h	2	3	5

Table 1. Serum samples were collected from surviving subjects at baseline, 24 hours, 48 hours, and 72 hours. Thirty-nine samples were collected in total.

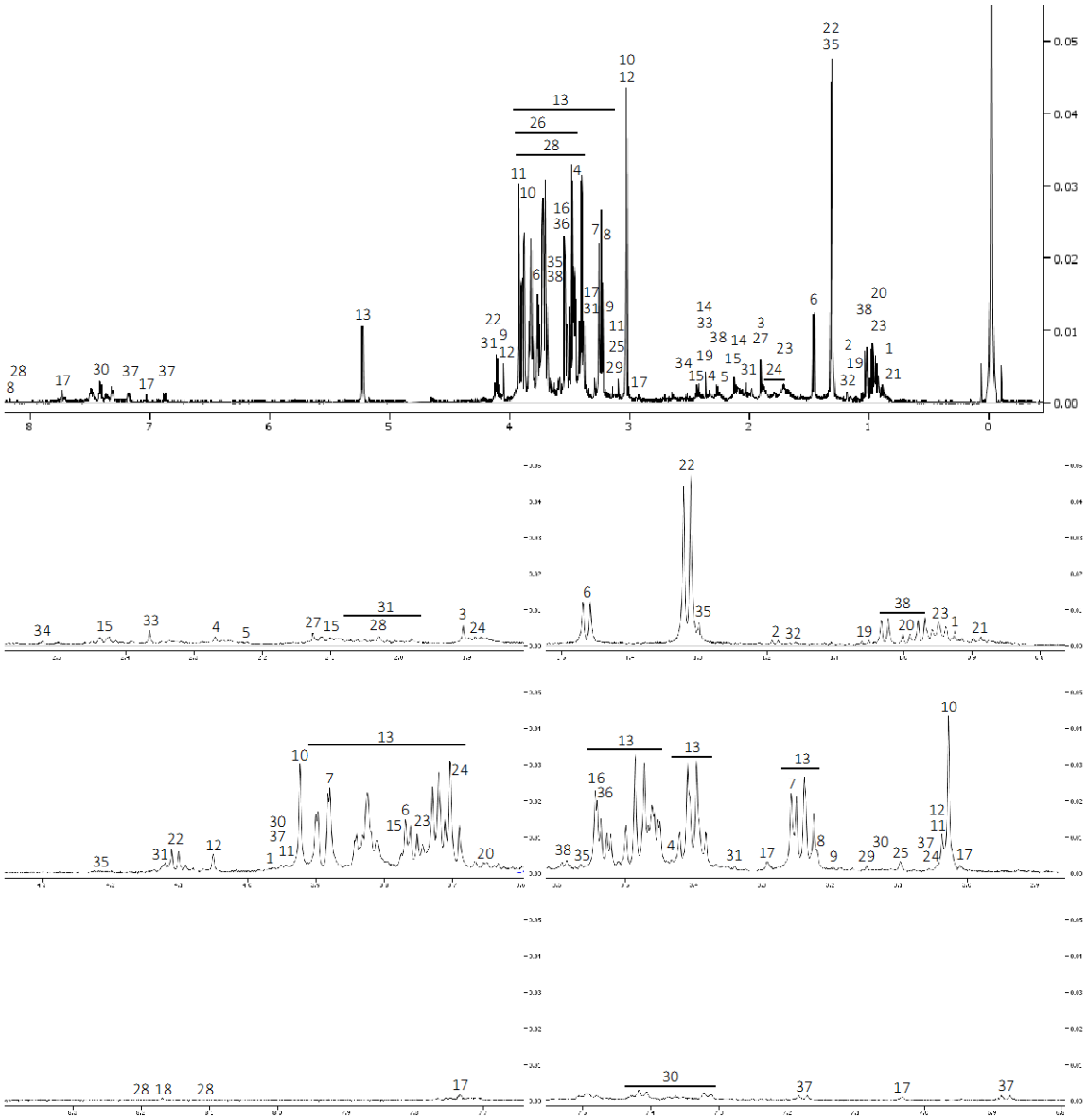

Figure 4. Known peaks from the Chenomx database were matched to ^{1}H-NMR spectra to obtain concentration values relative to the internal standard TSP. Concentrations shown here were not adjusted for dilution or loss to filtration. Peaks are marked by metabolite number listed alphabetically as follows: 1) 2-hydroxybutyrate, 2) 3-hydroxybutyrate, 3) acetate, 4) acetoacetate, 5) acetone, 6) alanine, 7) betaine, 8) carnitine, 9) choline, 10) creatine, 11) creatine phosphate, 12) creatinine, 13) glucose, 14) glutamate, 15) glutamine, 16) glycine, 17) histamine, 18) hypoxanthine, 19) isobutyrate, 20) isoleucine, 21) isovalerate, 22) lactate, 23) leucine, 24) lysine, 25) malonate, 26) mannose, 27) methionine, 28) N-acetylglucosamine, 29) O-phosphocholine, 30) phenylalanine, 31) proline, 32) propylene glycol, 33) pyruvate, 34) succinate, 35) threonine, 36) trimethylamine-N-oxide, 37) tyrosine, 38) valine. Position on the x-axis is determined by chemical shift in parts per million (ppm). The spectrum depicted above was collected from subject 592 at 24-hours following burn injury.

2-Hydroxybutyrate	Isoleucine
3-Hydroxybutyrate	Isovalerate
Acetate	Lactate
Acetoacetate	Leucine
Acetone	Lysine
Alanine	Malonate
Betaine	Mannose
Carnitine	Methionine
Choline	N-Acetylglucosamine
Creatine	O-Phosphocholine
Creatine phosphate	Phenylalanine
Creatinine	Proline
Glucose	Propylene glycol
Glutamate	Pyruvate
Glutamine	Succinate
Glycine	Threonine
Histamine	Trimethylamine-N-oxide
Hypoxanthine	Tyrosine
Isobutyrate	Valine

Table 2. 38 metabolites were identified using ^{1}H-NMR, listed alphabetically above.

Principal Component Analysis

PCA captured 51.6% of metabolite concentration variability in the first two principal components. Principal component 1 (PC1) accounted for 30.8% of variability, while principal component 2 (PC2) accounted for 20.8% of variability. 21 metabolites contributed more than average (2.63%) to the variability captured in the two-component model (Figure 5).

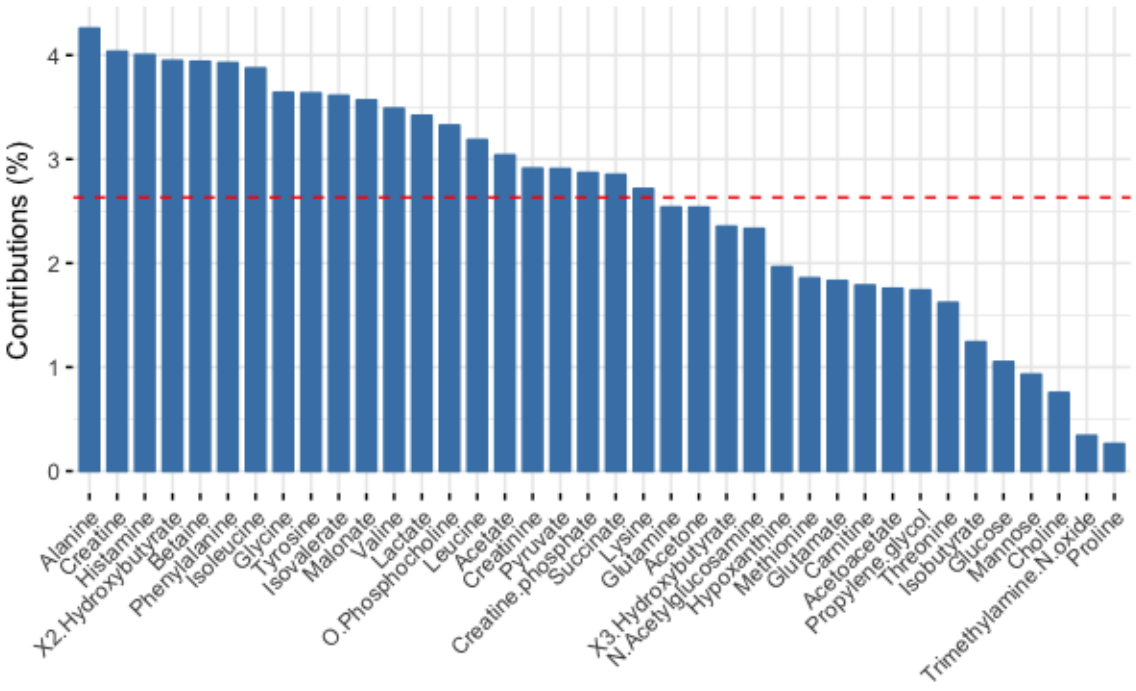

Figure 5. Metabolites were ranked according to the following formula: [(contrib.1*eig.1)+(contrib.2*eig.1)]/(eig.1*eig.2) where "contrib" specifies the contribution of that metabolite to a specific principal component, calculated as the square of the loadings vector, and "eig" specifies the eigenvalue of a specific principal component (39). The dashed line designates the average amount of variability each metabolite contributed to overall variability captured in the model. Metabolites with bars taller than the red line contributed more than average, while metabolites with bars shorter than the red line contributed less.

Hemoadsorption vs Sham Treatment

PCA scores showed extensive overlap of sample clusters based on treatment group (Figure 6). Kruskal-Wallis testing did not reveal significant differences ($p<0.05$) in the concentrations of any individual metabolites between treatment groups. Baseline samples were removed prior to both analyses due to protocol similarity preceding burn treatment. Based on the overlap of sample clusters by treatment group in PCA (Figure 6) and the lack of significant differences in individual metabolite concentrations between treatment groups according to Kruskal-Wallis testing, we concluded hemoadsorption treatment did

not have significant effects on the metabolomes of porcine burn subjects. Linden *et al.* also reported non-significant differences ($p>0.05$) in survival (hours after injury) between treatment groups (25). We therefore pooled subjects from both treatment groups for further analysis by time point.

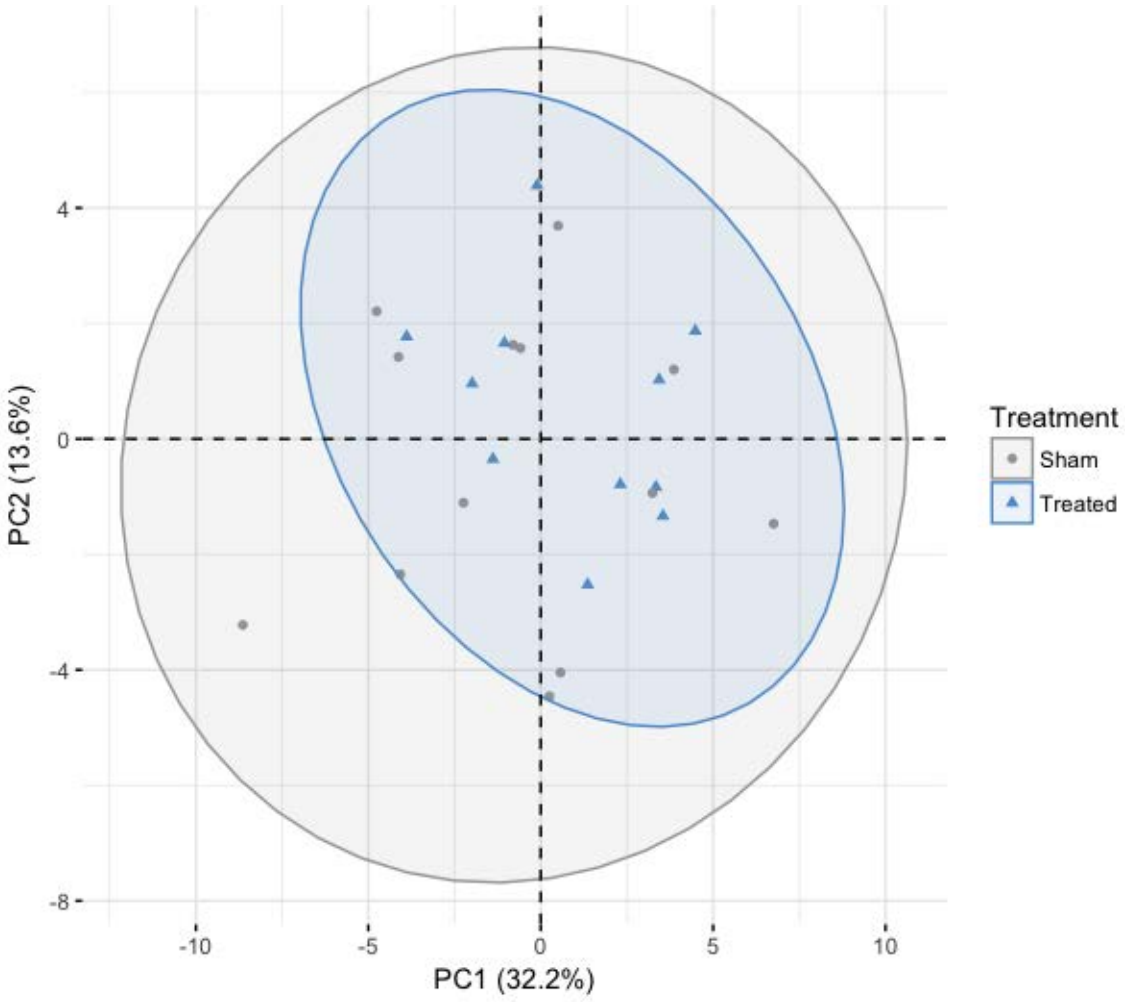

Figure 6. Principal component scores for components 1 (PC1) and 2 (PC2) were plotted for each sample. Sample points were then designated by treatment group and confidence intervals were drawn around a mean point for each group. Overlap of the confidence intervals signifies the variability of metabolite concentrations in each group was similarly patterned. Baseline samples were excluded due to protocol similarity prior to burn treatment.

Time Point Analysis

PCA scores showed distinct clustering and separation of samples from each time point based on two components (Figure 7). Kruskal-Wallis testing revealed significant concentration changes ($p<0.05$) in 31 of 38 metabolites during the 72-hour period (Table 3). Eighteen metabolite trends remained significant following Bonferonni multiple test correction ($p<0.0013$). Separation of sample clusters based on time point group in PCA (Figure 7) indicated each time point was characterized by a unique metabolic fingerprint. Ranked contributions of each metabolite to the variability captured in the PCA model (Figure 5) further indicated which metabolites contributed most to sample separation in that model. Combined with contribution vectors included in the PCA bi-plot of scores and contributions, we concluded alanine, betaine, glycine, lactate, and succinate contributed most to baseline (0h) sample character (Figure 8). Creatinine, histamine, and leucine contributed most to 24-hour sample character (Figure 9). Tyrosine, phenylalanine, creatine, 2-hydroxybutyrate, 3-hydroxybutyrate, isovalerate, acetone, acetoacetate, and propylene glycol contributed most to 48- and 72-hour sample character (Figure 10).

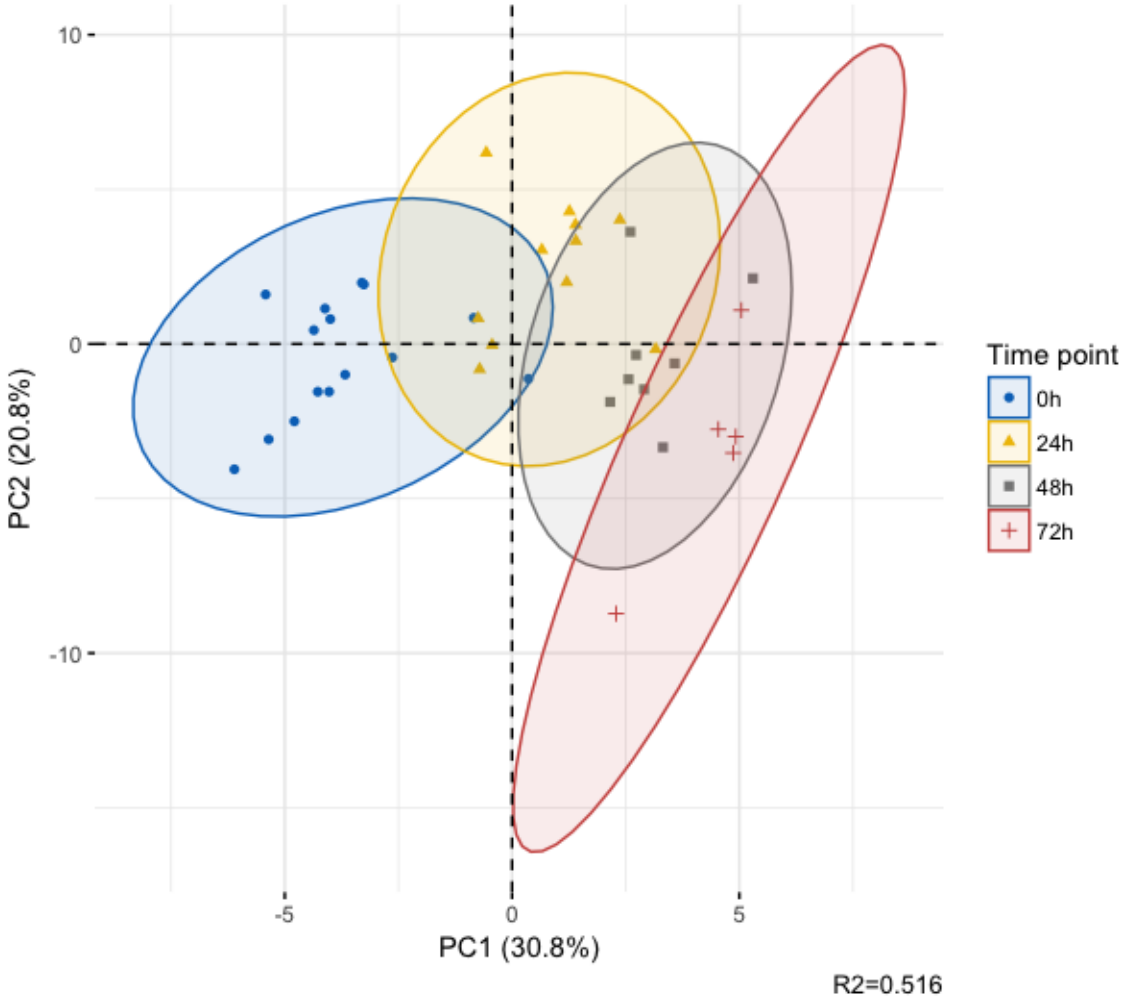

Figure 7. Principal component scores for components 1 (PC1) and 2 (PC2) were plotted for each sample. Sample points were then designated by time point group and confidence intervals were drawn around a mean point for each group. Clustering of samples by time point indicates patterns of metabolite concentration variability in the serum were characteristic of those time point groups. Contributions by each variable to separation and clustering in this model can be seen in Figure 5.

Metabolite	KW p-value	Metabolite	KW p-value
Alanine	**0.0001**	**Succinate**	**0.0005**
Creatine	**<0.0001**	Lysine	0.0034
Histamine	**0.0003**	Glutamine	0.0110
2-Hydroxybutyrate	**0.0001**	**Acetone**	**0.0011**
Betaine	**<0.0001**	3-Hydroxybutyrate	0.0037
Phenylalanine	**0.0001**	N-Acetylglucosamine	0.0052
Isoleucine	**0.0001**	Hypoxanthine	0.0157
Glycine	**<0.0001**	Methionine	0.0044
Tyrosine	**0.0001**	Glutamate	0.1199
Isovalerate	**0.0002**	Carnitine	0.0136
Malonate	**0.0001**	Acetoacetate	0.0306
Valine	0.0033	Propylene glycol	0.0033
Lactate	**<0.0001**	Threonine	0.3195
O-Phosphocholine	**0.0011**	Isobutyrate	0.0983
Leucine	0.0341	Glucose	0.1613
Acetate	**<0.0001**	**Mannose**	**0.0006**
Creatinine	0.0025	Choline	0.6691
Pyruvate	**0.0001**	Trimethylamine-N-oxide	0.7573
Creatine phosphate	0.0195	Proline	0.1769

Table 3. The significance of individual metabolite concentration trends was calculated with Kruskal-Wallis testing. Significance was accepted when $p<0.05$. Bold metabolites had concentration changes that remained significant following Bonferonni multiple test correction ($p<0.0013$). Metabolites are ordered by contribution to variability as shown in Figure 5.

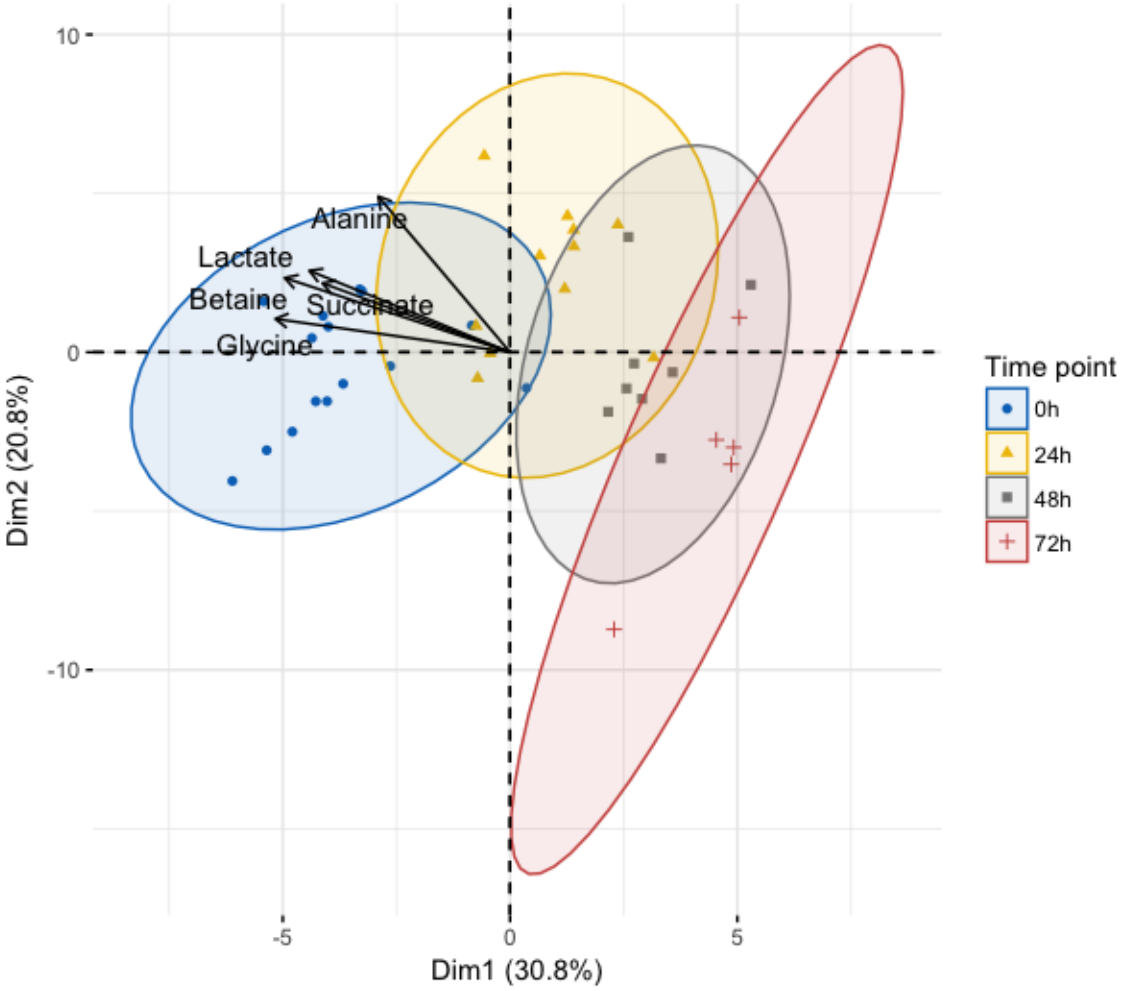

Figure 8. Contributions of metabolites most relevant to baseline (0h) sample character were superimposed over scores for each serum sample. The direction and magnitude of the contribution vectors indicated the trends of those metabolites were more strongly related to baseline (0h) sample character than to the character of samples from other time points.

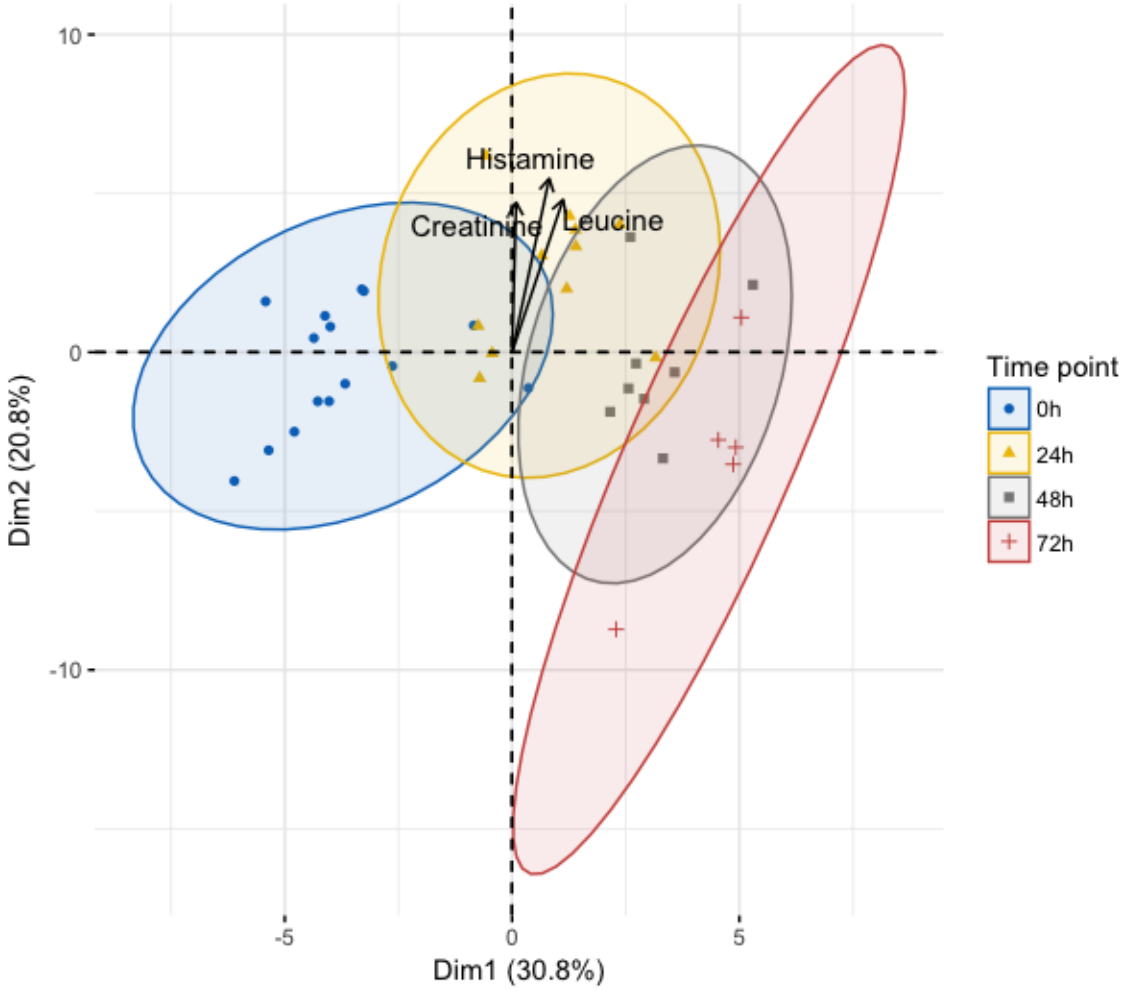

Figure 9. Contributions of metabolites most relevant to 24-hour sample character were superimposed over the two-dimensional scores plot for each serum sample. The direction and magnitude of the contribution vectors indicated the trends of those metabolites were more strongly related to 24-hour sample character than to the character of samples from other time points.

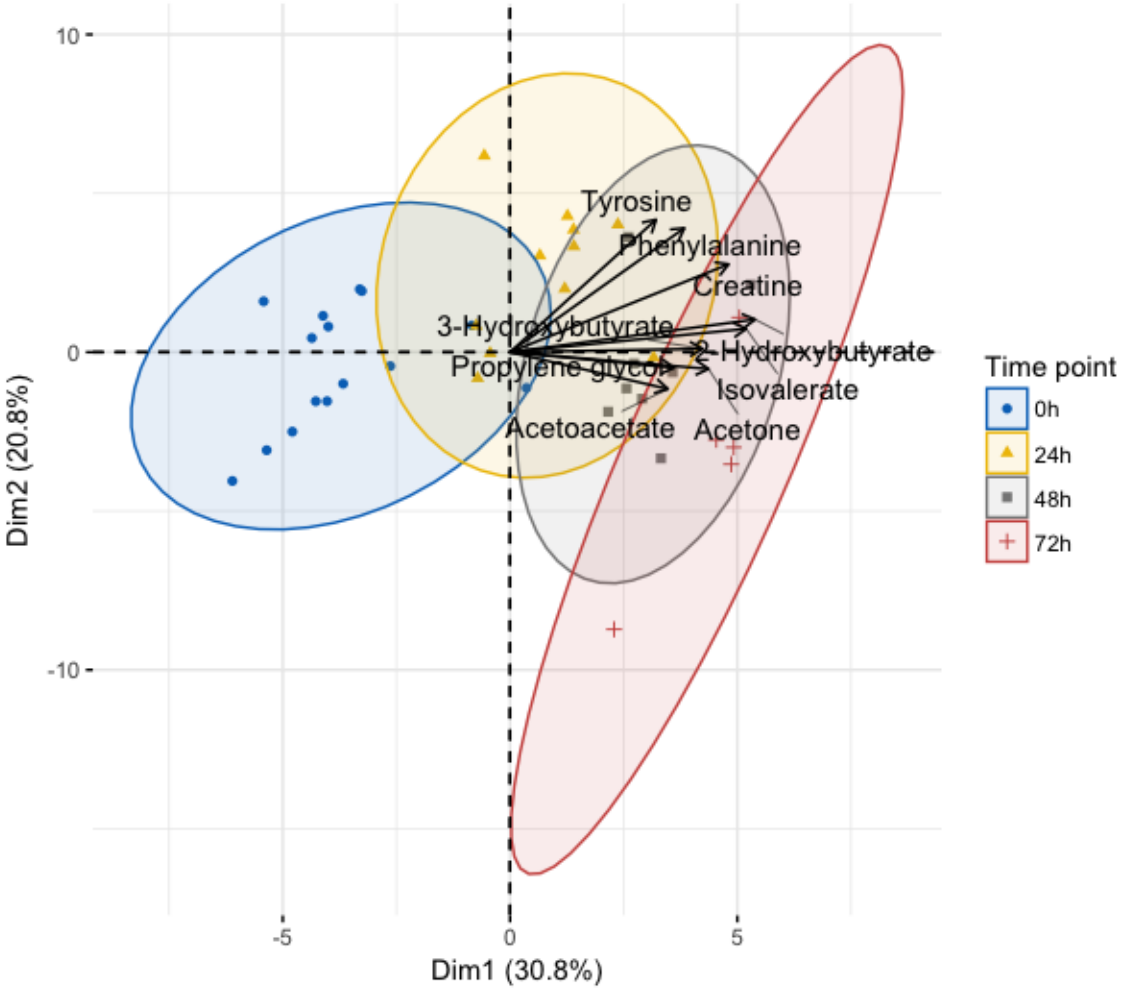

Figure 10. Contributions of metabolites most relevant to 48- and 72-hour sample character were superimposed over the two-dimensional scores plot for each serum sample. The direction and magnitude of the contribution vectors indicated the trends of those metabolites were more strongly related to 48- and 72-hour sample character than to the character of samples from other time points.

Arterial Blood Gas Data

Blood gas data included pH, serum lactate, base excess (BE), and blood urea nitrogen (BUN). Kruskal-Wallis testing showed significant changes in serum lactate ($p<0.001$), BE ($p=0.006$), BUN ($p<0.001$), and pH ($p<0.001$) during the 72-hour period. Serum lactate and pH were generally decreasing, while BE showed a mixed trend (Figure 11).

Pearson correlation revealed a positive relationship between pH and serum lactate (R^2=0.476, p=0.002) and a positive relationship between pH and BE (R^2=0.465, p=0.003), but there was not a significant correlation between lactate and BE (R^2=-0.062, p=0.708) (Figure 12). BUN was negatively correlated with pH (R^2=-0.694, p<0.001), serum lactate (R^2=-0.327, p=0.045), and BE (R^2=-0.349, p=0.032), respectively.

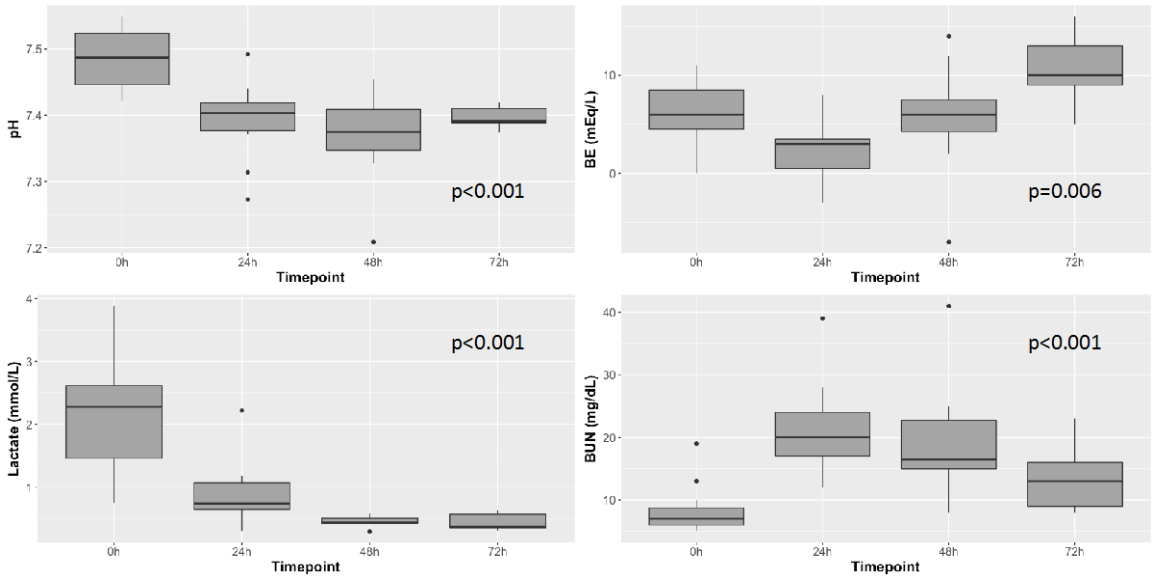

Figure 11. Kruskal-Wallis testing determined all blood gas variables changed significantly over time (p<0.05). Box plots were created using values for the median and interquartile range of each variable at each time point.

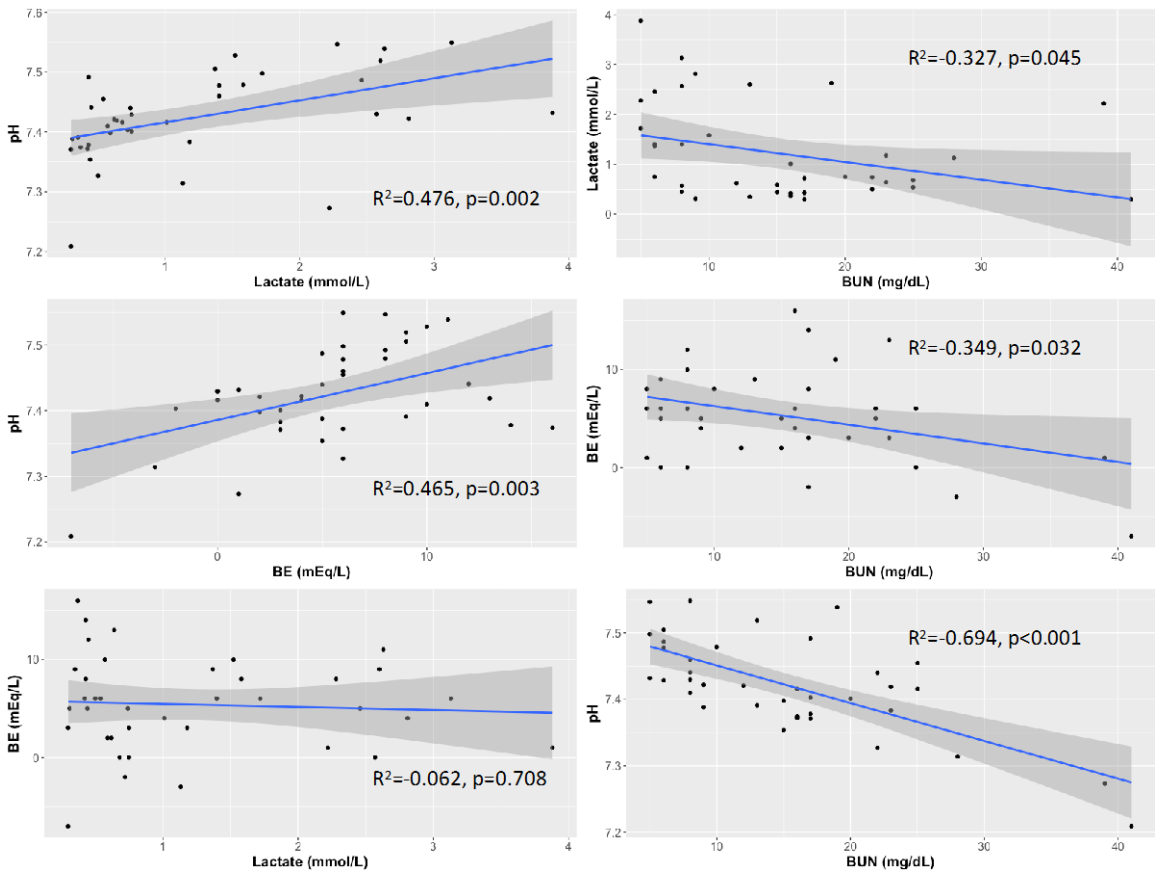

Figure 12. Pearson correlation determined the pairwise relationships between blood gas variables. Comparisons of lactate vs pH and BE vs pH showed significant, positive correlations ($p<0.05$). Comparisons of BUN vs lactate, BE vs BUN, and pH vs BUN showed significant, negative correlations ($p<0.05$). There was no significant relationship between BE and serum lactate ($p>0.05$).

CHAPTER 4

DISCUSSION AND CONCLUSIONS

As stated in the introduction, the goal of this study was to separate subject metabolomes by post-burn time point and characterize the transition between "ebb" and "flow" in post-burn metabolism. To accomplish that goal, we used ^{1}H-NMR spectroscopy to study samples of pig serum from baseline and three separate time points following a severe burn injury with additional smoke inhalation treatment. Two-dimensional principal component analysis (PCA) clearly separated samples from each time point into distinct groups based on overall variability patterns in their NMR profiles. By delving into the concentration changes of certain metabolites over time, and by examining the contributions they made to group separation in the two-component PCA model, we were able to identify key trends that characterized the metabolic transition from early (baseline, 24h) to late (48h, 72h) post-burn time points in our subjects.

Burn Shock and Resuscitation

Shock generally resolves within 24-48 hours of burn injury, or whenever an appropriate endpoint of resuscitation is reached (40). Hypermetabolism can begin to mount once the patient is fully resuscitated and hemodynamically stabilized. Reports that histamine levels begin to normalize by 36-hours after injury are consistent with the 24-hour histamine peak we observed in this study ($p<0.001$, Figure 13). Histamine is a key driver of hypovolemia in burn injury, as it weakens the tight junctions between vascular epithelial cells and allows intravascular fluids to exit into the interstitial space (41).

Histamine was also a primary contributor to 24-hour sample character based on its loadings vector in the PCA bi-plot (Figure 9). For our purposes, therefore, the time between the 24- and 48- hour time points presented a reasonable estimate for when the transition to the “flow” phase of recovery should begin. This was substantiated by the trends we observed in phenylalanine ($p<0.001$) and tyrosine ($p<0.001$) (Figure 13), which undergo increased cycling to maintain catecholamine levels in response to burn injury (42). Both phenylalanine and tyrosine increased significantly at the 24-hour time point and then decreased through 72 hours. They also contributed to the character of both 24-hour and 48-hour samples according to bi-plot analysis (Figure 10). Likely, these amino acids were released to accommodate the early catecholamine response and were subsequently converted into epinephrine and dopamine, decreasing their late-time point concentrations.

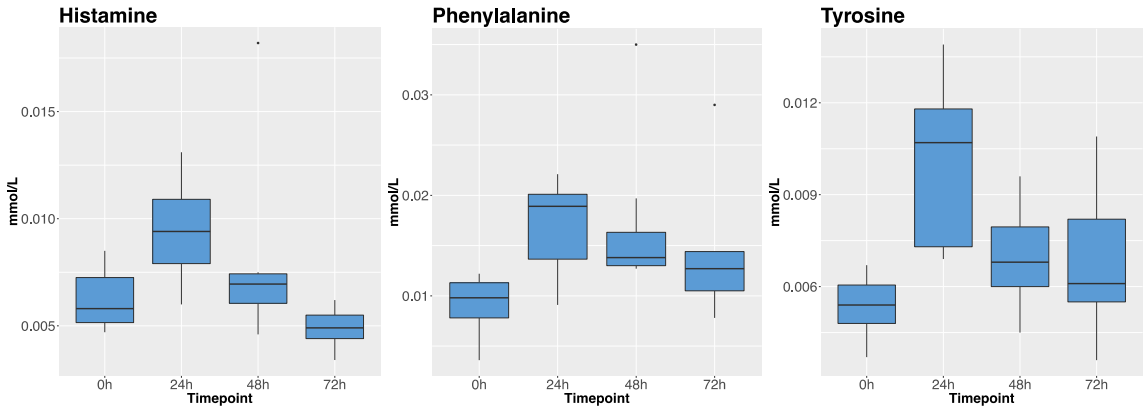

Figure 13. Box plots visualizing concentration trends for histamine ($p<0.001$), phenylalanine ($p<0.001$), and tyrosine ($p<0.001$) were created using concentration values for the median and interquartile range at each time point.

We observed decreasing concentrations of lactate ($p<0.001$) and succinate ($p<0.001$) at all time points in this study (Figure 14), indicating that hypoxia was not a significant contributor to post-burn metabolism even by the first post-burn time point. Decreasing betaine ($p<0.001$), glycine ($p<0.001$), and alanine ($p<0.001$) concentrations also strongly represented the character of baseline samples based on scores and contribution vectors (Figure 8). Alanine, as previously mentioned, is the primary amino acid shuttle that brings protein carbons to the liver for gluconeogenesis (8). The small peak we observed in alanine concentrations at 24 hours could reflect increased alanine release from skeletal muscle, but consumption of alanine must have outweighed its release at subsequent time points. Glycine has a similar capacity to alanine as an amino acid shuttle in the serum, and the decreasing concentrations we observed indicate glycine was progressively removed from circulation through 72 hours (43). Betaine should be produced as part of the transsulfuration pathway converting methionine to homocysteine, but we observed a converse depletion of betaine concentrations over time (44). The larger meaning of these trends is difficult to interpret without flux analysis utilizing labeled substrates.

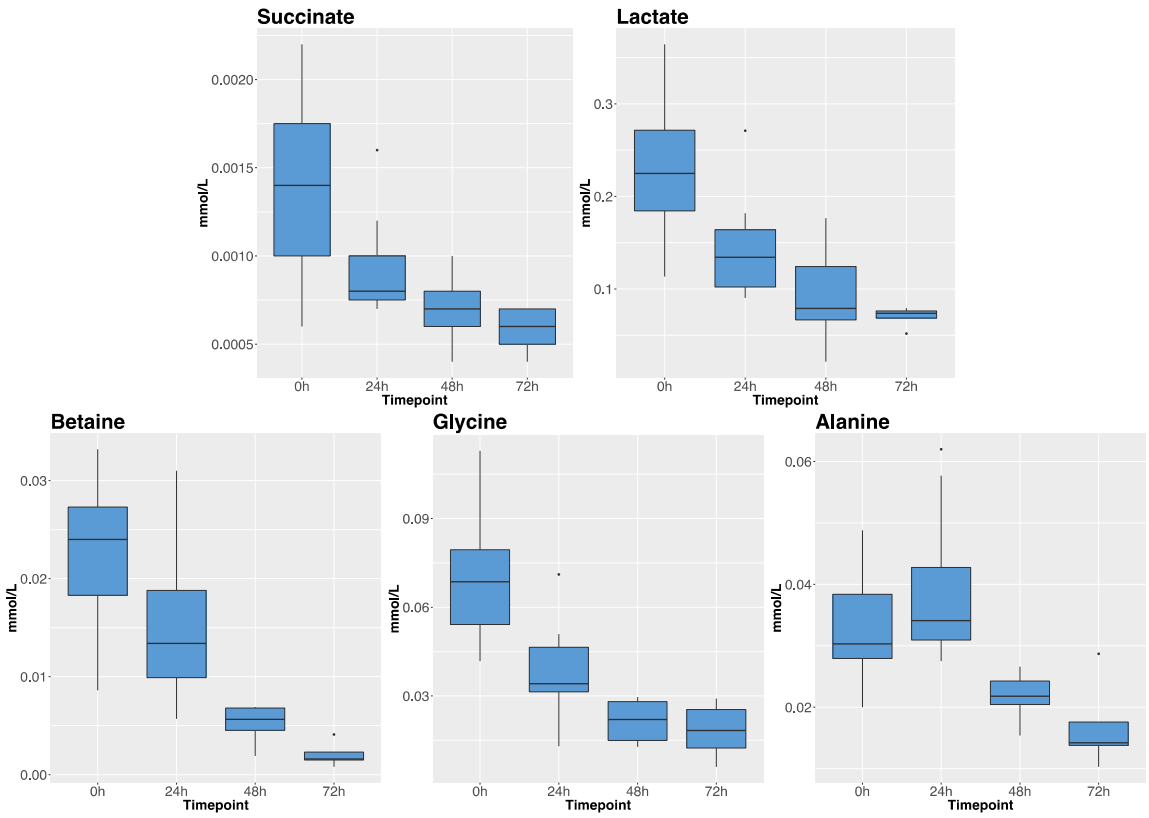

Figure 14. Box plots visualizing concentration trends for succinate ($p<0.001$), lactate ($p<0.001$), betaine ($p<0.001$), glycine ($p<0.001$), and alanine ($p<0.001$) were created using concentration values for the median and interquartile range at each time point.

Post-Resuscitation Metabolic Acidosis and Oxidative Stress

Among our most significant findings, we noted acidosis ($p<0.001$) in our subjects despite steady lactate clearance through 72 hours ($p<0.001$) (Figure 11). BE and BUN trends relative to serum pH further indicated a metabolic acidosis, and the lack of correlation between lactate and BE ($p=0.708$) indicated the observed acidosis was caused by accumulation of non-lactate anions following resuscitation in our subjects (Figure 12). As such, we sought to identify alternate sources of acidosis in our model to account for serum acidification without lactic acidemia. Four organic carboxylates (2-hydroxybutyrate, isovalerate, acetoacetate, 3-hydroxybutyrate) stood out as acidic species

that increased in concentration consistently from baseline to 72 hours. The PCA bi-plot of scores and contribution vectors (Figure 15) further indicated these organic carboxylates strongly characterized late-time point (48h, 72h) sample character. With help from the existing burn literature, we constructed a framework for persistent, non-lactate acidosis in severe burn victims that emphasizes post-resuscitation oxidative stress and fatty acid breakdown in response to post-burn adrenergic signaling (Figure 16).

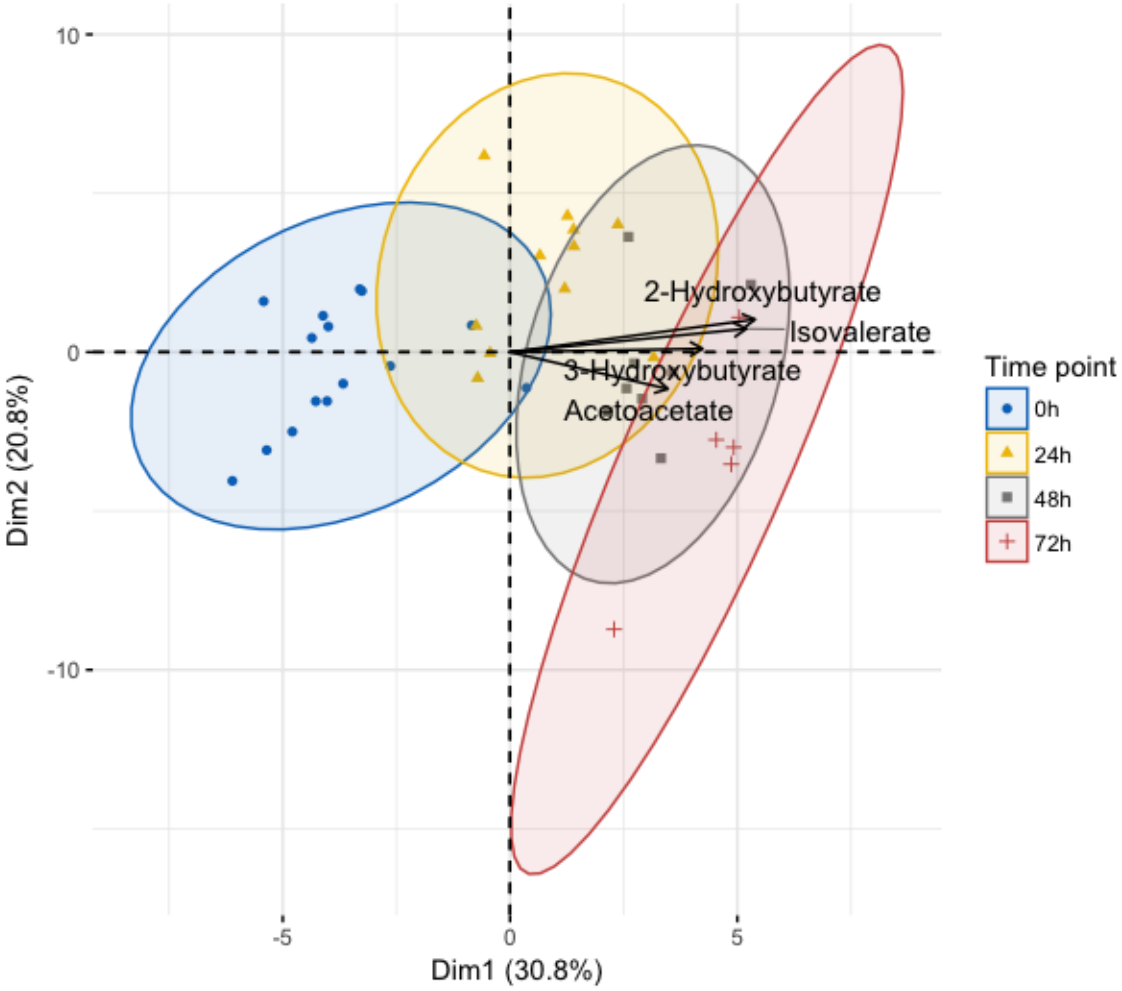

Figure 15. Contribution vectors for 2-hydroxybutyrate, isovalerate, acetoacetate, and 3-hydroxybutyrate were superimposed over the two-dimensional scores plot for each serum sample. The direction and magnitude of the contribution vectors indicated the trends of

those metabolites were more strongly related to 48- and 72-hour sample character than to the character of samples from other time points.

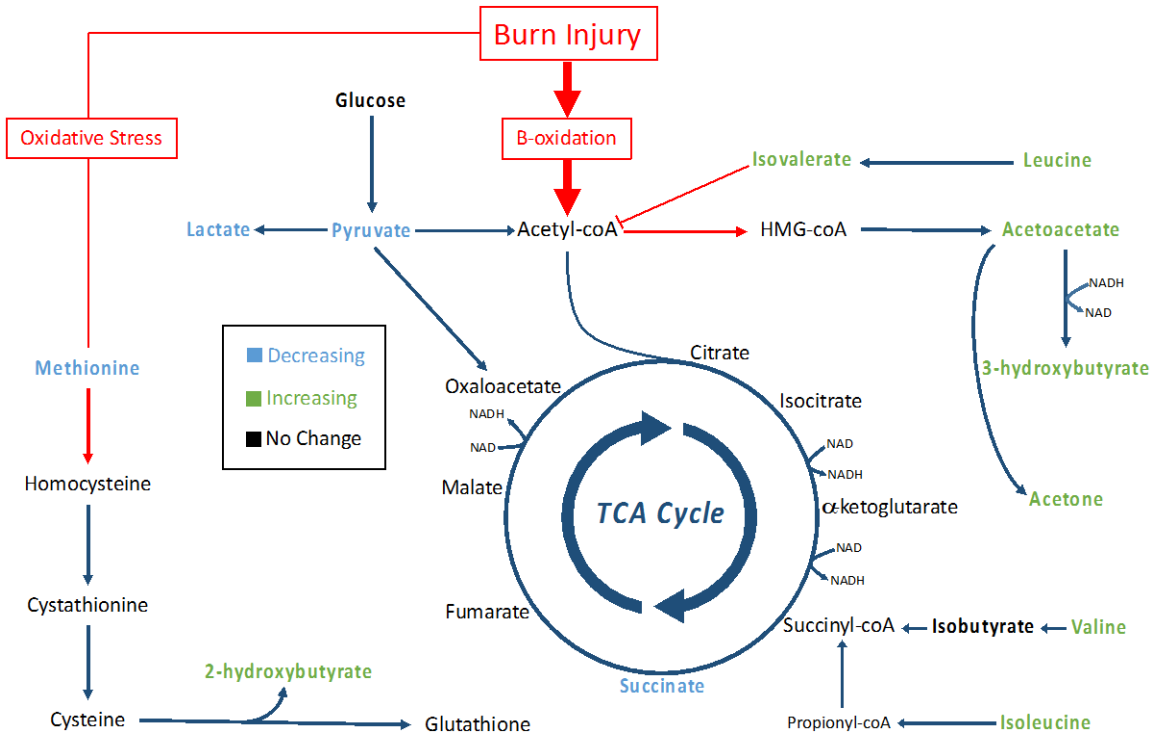

Figure 16. Pathways for ketogenesis, the TCA cycle, and transsulfuration for glutathione synthesis were outlined with focus on metabolites identified by in our analysis (bold). Green metabolites had significantly increasing concentration trends ($p<0.05$). Blue metabolites had significantly decreasing concentration trends ($p<0.05$). Black metabolites did not change concentration significantly ($p<0.05$), and non-bolded metabolites were not identified in our analysis. The red arrows and boxes represent possible aberrations due to burn injury that could have resulted in accumulation of 2-hydroxybutyrate, isovalerate, acetoacetate, and 3-hydroxybutyrate.

Oxidative Stress Metabolism

2-hydroxybutyrate (Figure 17) was the fourth most significant contributor to group separation in our two-component PCA model (Figure 5). Analysis of the bi-plot showed 2-hydroxybutyrate was also a significant contributor to 72-hour sample character based on the direction and magnitude of its loadings vector (Figure 15). We therefore concluded 2-hydroxybutyrate accumulation ($p<0.001$) became an increasingly prominent metabolic

feature as burn physiology progressed from resuscitation into hypermetabolism. This was likely due to oxidative stress that resulted once perfusion was restored to tissues that were in a state of hypoxia (45). 2-hydroxybutyrate is produced during the synthesis of cysteine, which is needed to sustain increased glutathione cycling during times of high oxidative stress (46). Furthermore, the homocysteine precursor for cysteine production is shunted away from methionine synthesis, which was reflected by the decreasing methionine concentrations we observed following resuscitation (p=0.004). Finally, increasing hypoxanthine concentrations (p=0.016) through 48 hours provided a direct indication of oxidative stress following resuscitation in this model. Hypoxanthine is converted to xanthine by xanthine oxidase for excretion as uric acid, producing hydrogen peroxide as a byproduct (47). Xanthine oxidase activity increases following burn injury, and increased serum hypoxanthine levels have been used as indicators of oxidative stress in previous studies (48). Taken together, these concentration trends indicated oxidative stress following burn injury produced 2-hydroxybutyrate as a byproduct of increased glutathione synthesis, leading to 2-hydroxybutyric acidosis.

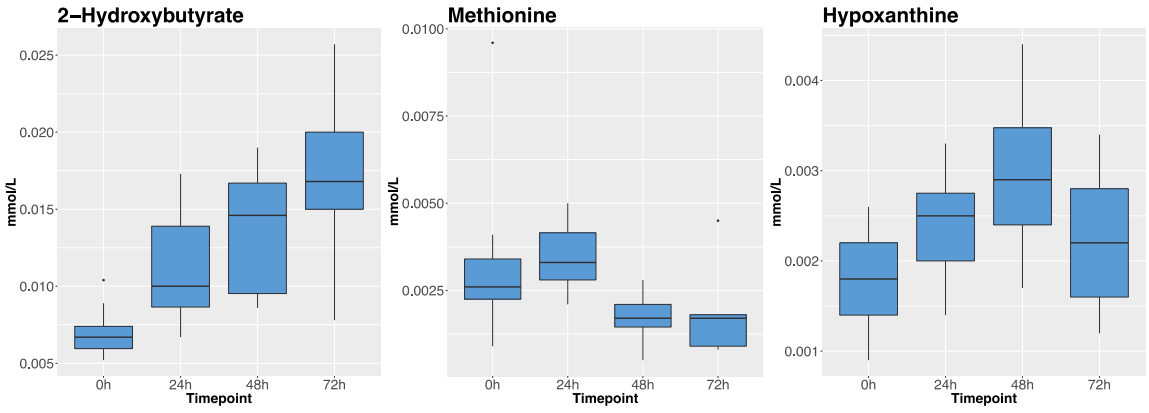

Figure 17. Box plots visualizing concentration trends for 2-hydroxybutyrate ($p<0.001$), methionine ($p=0.004$), and hypoxanthine ($p=0.016$) were created using concentration values for the median and interquartile range at each time point.

Branched Chain Amino Acid Catabolism

Isovalerate accumulation also contributed significantly to the character of 48- and 72-hour samples in our two-component PCA model (Figure 15) and had an increasing concentration trend through 72 hours ($p<0.001$, Figure 18). Isovalerate is an intermediate of leucine metabolism that is known to accumulate in the blood with conditions of incomplete leucine breakdown (49). We also noted that isobutyrate, the analog to isovalerate in valine catabolism, did not show significant concentration changes during the study period ($p=0.098$). We took this to indicate leucine catabolism was disturbed following burn injury while valine catabolism proceeded unchanged. A key difference between leucine and valine metabolism that could explain this discrepancy is that leucine is ketogenic and valine is glucogenic, meaning isovalerate enters the TCA cycle as acetyl-coA and isobutyrate enters the cycle as succinyl-coA (50). We propose that, under conditions of high acetyl-coA production such as those following burn injury, conversion of isovalerate to acetyl-coA is inhibited while isobutyrate conversion to succinyl-coA continues unaffected. This results in isovaleric acidosis in resuscitated burn victims due to an abundance of acetyl-coA, likely originating from high levels of post-burn adrenergic β-oxidation.

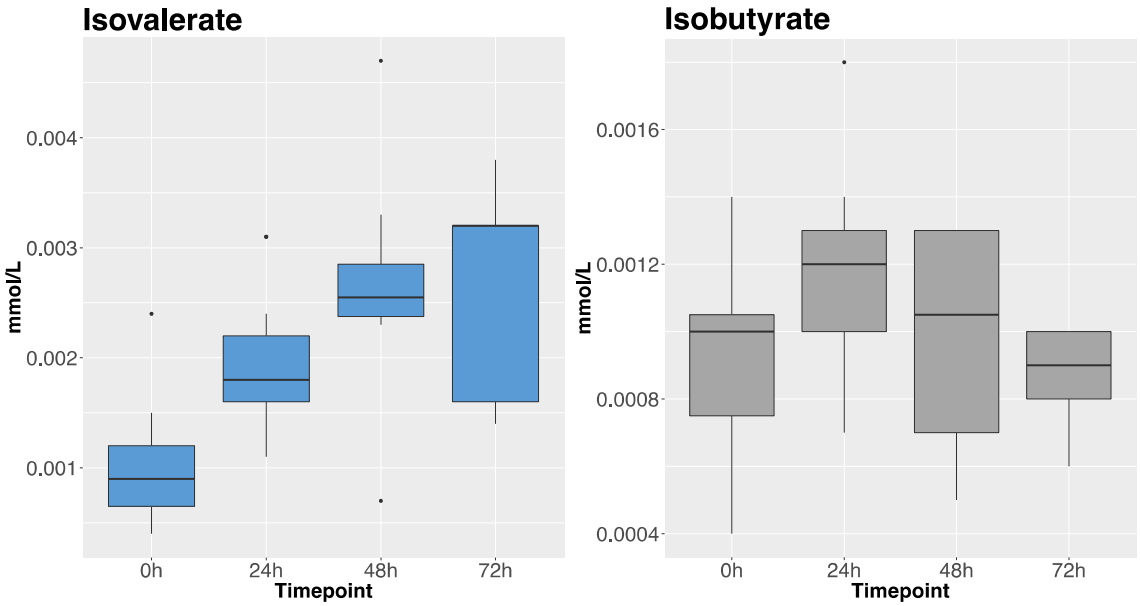

Figure 18. Box plots visualizing concentration trends for isovalerate ($p<0.001$) and isobutyrate ($p=0.098$) were created using concentration values for the median and interquartile range at each time point.

Ketone Body Metabolism

Acetoacetate and 3-hydroxybutyrate both showed significantly increasing concentration trends ($p=0.031$, 0.004, Figure 19) and contributed to late-time point sample character in the PCA bi-plot (Figure 15). Acetone also increased significantly ($p=0.001$), but it is not an acidic compound. Acetoacetate and 3-hydroxybutyrate are ketone bodies used by vital organs during times of metabolic stress or increased fatty acid catabolism. Acetone is a breakdown product of the other two ketone bodies. In diabetes, accumulation of ketone bodies occurs due to the effects of insulin resistance and increased dependence on fats as fuels (51). In starvation, ketosis occurs because carbohydrate stores are depleted and fats become the major remaining fuel source to support organ function (52). Burn injury combines these two etiologies, where the early "fight-or-flight" response depletes glycogen stores and causes insulin resistance in skeletal muscle cells. It is widely known

that burn victims are high-risk populations for malnutrition and morbidities such as ketoacidosis due to the high level of metabolic stress burn injuries cause.

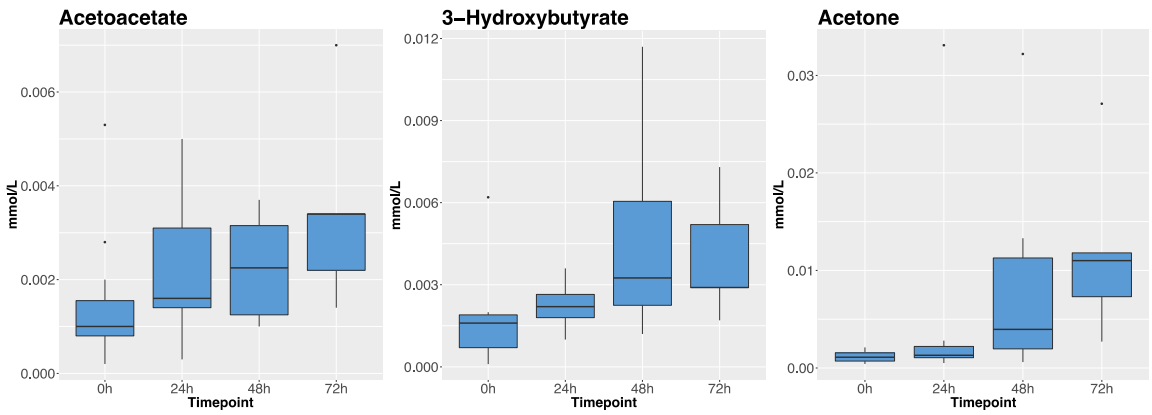

Figure 19. Box plots visualizing concentration trends for acetoacetate (p=0.031) and 3-hydroxybutyrate (p=0.004), and acetone (p=0.001) were created using concentration values for the median and interquartile range at each time point.

Other Acidic Contributors

Other possible contributors to acidosis in this model included propylene glycol and malonate. Propylene glycol is a pharmaceutical solvent that increased in concentration through 72 hours in our subjects (p=0.003, Figure 20), likely due to continuous drug administration. However, propylene glycol causes acidosis through its breakdown into lactic acid (53), so decreasing lactate concentrations make propylene glycol an unlikely source of acidosis, and certainly not a source of non-lactate acidosis, in our model. Serum malonate concentrations increased through 24 hours, after which time they decreased past baseline through 72 hours (p<0.001). Malonate therefore could have been an early contributor to acidosis that resolved with a slight lag following resuscitation. However, there is little published about mammalian production of malonate other than that it

accumulates with deficiencies of malonyl-coA decarboxylase, an enzyme that converts malonyl-coA to actetyl-coA to promote increased β-oxidation (54). Another metabolite involved in the regulation of β-oxidation, carnitine, followed a similar pattern to malonate (p=0.014). It is intriguing to consider the relationship between carnitine and malonate concentrations following burn injury, but conclusions cannot be drawn from this analysis. Malonate, malonyl-coA, and carnitine therefore should be studied further to identify pathways that could be relevant to the understanding of burn metabolism.

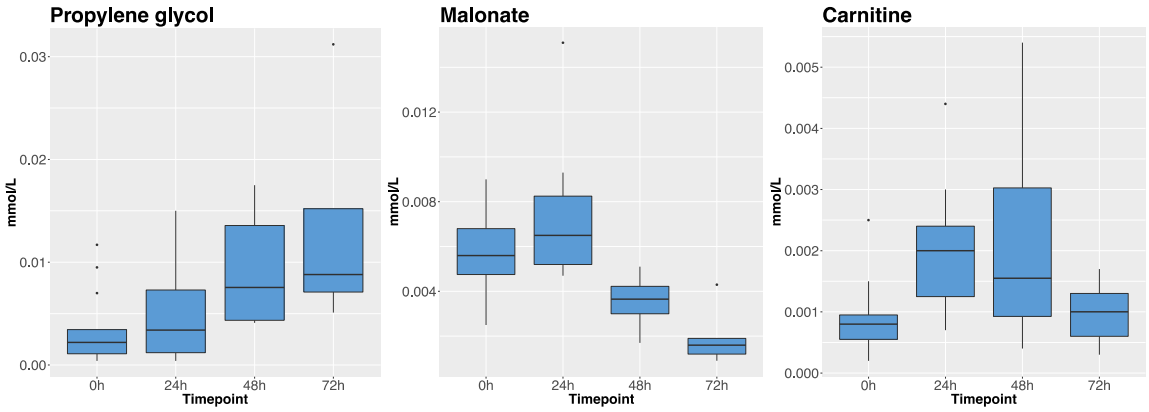

Figure 20. Box plots visualizing concentration trends for propylene glycol (p=0.003), malonate (p<0.001), and carnitine (p=0.014) were created using concentration values for the median and interquartile range at each time point.

Smoke Inhalation Injury

No obvious effects attributable to smoke inhalation injury alone were observed. This would be a good target for a controlled metabolomic study comparing subjects receiving burn injury with and without smoke inhalation in the future.

Study Weaknesses and Limitations

Elevated lactate at baseline suggested subjects might have had a pre-existing response to surgical trauma before burn trauma was introduced. Optimal controls were also not available due to the secondary nature of this analysis. Lack of controls made it difficult to determine, for example, what amount of acidosis in our subjects was due to the animals' fasting status and what was due to burn alone. An ideal trial would control for nutrition and include a resting period following tracheostomy and cannulation to minimize the influence of surgical trauma on experimental results.

The number of subjects was low in this trial, especially at later time points due to subject mortality. Increasing the number of trial participants would increase the power of analysis. Though increasing the number of participants would make the study more powerful, a larger trial would also require appropriate scaling of controls. To solve the problem of cost with larger subject pools in future studies, it seems reasonable to use clinical samples from human subjects given volume of blood needed for each sample. Using human subjects in the future would eliminate the physiological gap between animal models and human subjects, and would allow for continuous enrollment of new subjects into the study.

The number of metabolites we identified was relatively low, which might be due to the sensitivity of the NMR platform in comparison to mass spectrometry. Use of mass spectrometry could identify more features at lower concentrations and it could potentially fill the metabolic gaps in our pathway analysis. Preparations of the lipid phase in addition

to the aqueous phase of each sample using either NMR or mass spectrometry would also increase the number of metabolites available for analysis. Lipid data could be very useful, as much of burn metabolism is fueled by lipid breakdown. In addition, we did not quantify acetyl-coA and thus we are unable to verify our assertions concerning the consequences of increases in levels of this molecule.

Finally, though the sampling schedule provided for this study was well-dispersed around a 36-hour midpoint for "ebb" recovery (resolution of burn shock), more frequent sampling would increase the resolution of metabolite concentration trends. Perhaps most useful would be a 0h post-burn time point to indicate the immediate response to burn injury. Immediate post-burn sampling would likely show increases in lactate and succinate concentrations, for example, due to tissue hypoxia in burn shock. More informative still would be a pathway study where radio- or heavy-labeled metabolic isotopes could show flux of metabolites through metabolic pathways.

Future Directions

Much of the management of severe burn injury is focused on combating the effects of hypermetabolism. High-carbohydrate, high-protein diets are meant to minimize endogenous protein breakdown in hypermetabolic patients (55, 56). Metformin has been shown to improve peripheral glucose uptake in insulin resistant patients so they can more effectively utilize non-protein fuel sources (57). Blockade of β-adrenergic receptors in the pancreas has been shown to mitigate the overall hypermetabolic response to some extent (58, 59). However, it is likely that hypermetabolism is an adaptive response to

conditions that were once unsurvivable without the benefits of modern medicine. It is valuable to continue developing our understanding of burn physiology to understand how adaptive responses, such as inflammation and hypermetabolism, become detrimental to patient outcomes once injuries become too severe.

Conclusions

In this study, we used ^{1}H-NMR metabolomics to examine metabolic changes of porcine subjects during the first 72 hours after burn injury with additional smoke inhalation treatment. PCA of serum metabolites successfully separated samples from baseline and three post-burn time points using two principal components, and the vast majority of identified metabolites (31 of 38) showed significant concentration changes through 72 hours. Baseline samples were best characterized by high concentrations of succinate, lactate, alanine, betaine, and glycine, while 24-hour samples exhibited a prominent peak in histamine levels. Later time points were defined by cycling of the catecholamine precursor tyrosine and its parent phenylalanine, elevated markers of oxidative stress (2-hydroxybutyrate, hypoxanthine), and ketone metabolism (acetoacetate, 3-hydroxybutyrate, acetone). Interestingly, blood gas data also showed persistent acidosis despite consistent serum lactate clearance throughout the duration of the study. As such, we sought to identify alternate sources of acidosis in our porcine subjects to account for serum acidification without lactic acidemia. Four organic carboxylates (2-hydroxybutyrate, isovalerate, acetoacetate, 3-hydroxybutyrate) stood out as acidic species that consistently increased in concentration in the serum from baseline to 72 hours. These organic carboxylates contributed heavily late-time point (48h, 72h) sample character in

our two-component model. In summary, we have found post-burn metabolomes of porcine subjects to be easily distinguishable using ^{1}H-NMR and principal component analysis. We have also constructed a framework for non-lactate acidosis in resuscitated burn victims that emphasizes oxidative stress and increased fatty acid catabolism as root causes of organic acid accumulation. Further studies will be required to confirm and elaborate on the post-burn metabolic pathways suggested by this analysis.

CHAPTER 5

REFERENCES

1. Steel N. Global, regional, and national age-sex specific mortality for 264 causes of death, 1980–2016: a systematic analysis for the Global Burden of Disease Study 2016. Lancet. 2017;390(10100):1151-210.

2. Burn Incidence Fact Sheet: American Burn Association; 2016 [cited 2017]. Available from: http://ameriburn.org/who-we-are/media/burn-incidence-fact-sheet/.

3. Cuthbertson D. Post-shock metabolic response. The Lancet. 1942;239(6189):433-7.

4. Hatef DA, Hollier Jr LH. Pathophysiologic Response to Severe Burn Injury. Journal of Craniofacial Surgery. 2009;20(4):1300-1.

5. Rae L, Fidler P, Gibran N. The physiologic basis of burn shock and the need for aggressive fluid resuscitation. Critical care clinics. 2016;32(4):491-505.

6. Wilmore DW, Aulick LH. Metabolic changes in burned patients. The Surgical clinics of North America. 1978;58(6):1173-87.

7. Miller HI, Wolfe RR, Ferguson JL, Moss SW. Metabolic and Hemodynamic Aspects of the Hypothermia of Early Burn Shock. Effectors of Thermogenesis: Springer; 1978. p. 327-31.

8. Felig P. The glucose-alanine cycle. Metabolism-Clinical and Experimental. 1973;22(2):179-207.

9. Berg J, Tymoczko J, Stryer L. Section 16.3. Glucose can be-synthesized from noncarbohydrate precursors. Biochemistry. 2002:479-85.

10. Xiao W, Mindrinos MN, Seok J, Cuschieri J, Cuenca AG, Gao H, Hayden DL, Hennessy L, Moore EE, Minei JP. A genomic storm in critically injured humans. Journal of Experimental Medicine. 2011;208(13):2581-90.

11. Colohan SM. Predicting prognosis in thermal burns with associated inhalational injury: a systematic review of prognostic factors in adult burn victims. Journal of Burn Care & Research. 2010;31(4):529-39.

12. Shirani KZ, Pruitt Jr BA, Mason Jr AD. The influence of inhalation injury and pneumonia on burn mortality. Annals of surgery. 1987;205(1):82.

13. Dries DJ, Endorf FW. Inhalation injury: epidemiology, pathology, treatment strategies. Scandinavian journal of trauma, resuscitation and emergency medicine. 2013;21(1):31.

14. Sen S, Palmieri T, Greenhalgh D. Review of burn research for year 2014. Journal of Burn Care & Research. 2015;36(6):587-94.

15. Bathe OF, Farshidfar F. From genotype to functional phenotype: unraveling the metabolomic features of colorectal cancer. Genes. 2014;5(3):536-60.

16. Peltz ED, D'Alessandro A, Moore EE, Chin T, Silliman CC, Sauaia A, Hansen KC, Banerjee A. Pathologic metabolism: an exploratory study of the plasma metabolome of critical injury. The journal of trauma and acute care surgery. 2015;78(4):742.

17. Cohen MJ, Serkova NJ, Wiener-Kronish J, Pittet J-F, Niemann CU. 1H-NMR-based metabolic signatures of clinical outcomes in trauma patients—beyond lactate and base deficit. Journal of Trauma and Acute Care Surgery. 2010;69(1):31-40.

18. Lusczek ER, Muratore SL, Dubick MA, Beilman GJ. Assessment of key plasma metabolites in combat casualties. Journal of Trauma and Acute Care Surgery. 2017;82(2):309-16.

19. Parent BA, Seaton M, Sood RF, Gu H, Djukovic D, Raftery D, O'Keefe GE. Use of metabolomics to trend recovery and therapy after injury in critically ill trauma patients. JAMA surgery. 2016;151(7):e160853-e.

20. Yi L, Shi S, Wang Y, Huang W, Xia Z-a, Xing Z, Peng W, Wang Z. Serum metabolic profiling reveals altered metabolic pathways in patients with post-traumatic cognitive impairments. Scientific reports. 2016;6.

21. Blaise BJ, Gouel-Chéron Al, Floccard B, Monneret G, Allaouchiche B. Metabolic phenotyping of traumatized patients reveals a susceptibility to sepsis. Analytical chemistry. 2013;85(22):10850-5.

22. Zhang Y, Cai B, Jiang H, Yan H, Yang H, Peng J, Wang W, Ma S, Wu X, Peng X. Use of 1 H-nuclear magnetic resonance to screen a set of biomarkers for monitoring metabolic disturbances in severe burn patients. Critical care. 2014;18(4):R159.

23. Liu X-R, Zheng X-F, Ji S-Z, Lv Y-h, Zheng D-Y, Xia Z-F, Zhang W-D. Metabolomic analysis of thermally injured and/or septic rats. Burns. 2010;36(7):992-8.

24. Zang T, Broszczak DA, Broadbent JA, Cuttle L, Lu H, Parker TJ. The biochemistry of blister fluid from pediatric burn injuries: proteomics and metabolomics aspects. Expert review of proteomics. 2016;13(1):35-53.

25. Linden K, Scaravilli V, Kreyer SF, Belenkiy SM, Stewart IJ, Chung KK, Cancio LC, Batchinsky AI. Evaluation of the cytosorb™ hemoadsorptive column in a pig model of severe smoke and burn injury. Shock. 2015;44(5):487-95.

26. Derrell J, Baldwin R, Bayne K, Brown M, Gebhart G, Gonder J, Gwathmey J, Keeling M, Kohn D, Robb J. The Guide for the Care and Use of Laboratory Animals. Institute of laboratory animal resources Washington DC, USA. 1996.

27. Regulations AW. Animal Welfare Act. 2013.

28. Salinas J, Chung KK, Mann EA, Cancio LC, Kramer GC, Serio-Melvin ML, Renz EM, Wade CE, Wolf SE. Computerized decision support system improves fluid resuscitation following severe burns: an original study. Critical care medicine. 2011;39(9):2031-8.

29. AVMA Guidelines on Euthanasia. American Veterinary Medical Association; 2007.

30. Weljie AM, Newton J, Mercier P, Carlson E, Slupsky CM. Targeted profiling: quantitative analysis of 1H NMR metabolomics data. Analytical chemistry. 2006;78(13):4430-42.

31. Team RC. R: A Language and Environment for Statistical Computing. R Foundation for Statistical Computing; 2016.

32. Brereton RG, Lloyd GR. Partial least squares discriminant analysis: taking the magic away. Journal of Chemometrics. 2014;28(4):213-25.

33. Xia J, Wishart DS. Using MetaboAnalyst 3.0 for comprehensive metabolomics data analysis. Current protocols in bioinformatics. 2016:14.0. 1-.0. 91.

34. Chong J, Soufan O, Li C, Caraus I, Li S, Guillaume B, Wishart D, Xia J. MetaboAnalyst 4.0: towards more transparent and integrative metabolomics analysis. Nucleic Acids Research. 2018.

35. Sanchez G, Determan C. DiscriMiner: Tools of the Trade for Discriminant Analysis. 0.1-29 ed2013.

36. Husson F, Josse J, Le S, Mazet J. FactoMineR: An R Package for Multivariate Analysis (version 1.39). Journal of Statistical Software. 2008;25(1):1-18.

37. Kassambara A, Mundt F. factoextra: Extract and Visualize the Results of Multivariate Data Analyses (version 1.0.5). 2017.

38. Wickham H. ggplot2: Elegant Graphics for Data Analysis (version 2.2.1). Springer-Verlag New York; 2009.

39. PCA - Principal Component Analysis Essentials - Articles - STHDA 2018 [cited 2018]. Available from: http://www.sthda.com/english/articles/31-principal-component-methods-in-r-practical-guide/112-pca-principal-component-analysis-essentials/.

40. McNelis J, Marini CP, Jurkiewicz A, Szomstein S, Simms HH, Ritter G, Nathan IM. Prolonged lactate clearance is associated with increased mortality in the surgical intensive care unit. The American journal of surgery. 2001;182(5):481-5.

41. Carvajal HF, Brouhard BH, Linares HA. Effect of antihistamine-antiserotonin and ganglionic blocking agents upon increased capillary permeability following burn trauma. The Journal of trauma. 1975;15(11):969-75.

42. Herndon DN, Wilmore DW, Mason AD, Pruitt BA. Abnormalities of phenylalanine and tyrosine kinetics: Significance in septic and nonseptic burned patients. Archives of Surgery. 1978;113(2):133-5.

43. Askanazi J, Carpentier Y, Michelsen C, Elwyn D, Furst P, Kantrowitz L, Gump F, Kinney J. Muscle and plasma amino acids following injury: influence of intercurrent infection. Annals of surgery. 1980;192(1):78.

44. Witowski N, Lusczek E, Determan Jr C, Lexcen D, Mulier K, Ostrowski B, Beilman G. A four-compartment metabolomics analysis of the liver, muscle, serum, and urine response to polytrauma with hemorrhagic shock following carbohydrate prefeed. PloS one. 2015;10(4):e0124467.

45. Mulier KE, Lexcen DR, Luzcek E, Greenberg JJ, Beilman GJ. Treatment with beta-hydroxybutyrate and melatonin is associated with improved survival in a porcine model of hemorrhagic shock. Resuscitation. 2012;83(2):253-8.

46. Dash PK, Hergenroeder GW, Jeter CB, Choi HA, Kobori N, Moore AN. Traumatic brain injury alters methionine metabolism: implications for pathophysiology. Frontiers in systems neuroscience. 2016;10:36.

47. Tang H-J, Li W, Zhou M, Peng L-Y, Wang J-X, Li J-H, Chen J. Design, synthesis and biological evaluation of novel xanthine oxidase inhibitors bearing a 2-arylbenzo [b] furan scaffold. European journal of medicinal chemistry. 2018;151:849-60.

48. Jacob S, Herndon DN, Hawkins HK, Enkhbaatar P, Cox RA. Xanthine oxidase contributes to sustained airway epithelial oxidative stress after scald burn. International journal of burns and trauma. 2017;7(6):98.

49. Budd MA, Tanaka K, Holmes LB, Efron ML, Crawford JD, Isselbacher KJ. Isovaleric acidemia: clinical features of a new genetic defect of leucine metabolism. New England Journal of Medicine. 1967;277(7):321-7.

50. Harper A, Miller R, Block K. Branched-chain amino acid metabolism. Annual review of nutrition. 1984;4(1):409-54.

51. Usher-Smith JA, Thompson MJ, Sharp SJ, Walter FM. Factors associated with the presence of diabetic ketoacidosis at diagnosis of diabetes in children and young adults: a systematic review. Bmj. 2011;343:d4092.

52. Mostert M, Bonavia A. Starvation ketoacidosis as a cause of unexplained metabolic acidosis in the perioperative period. The American journal of case reports. 2016;17:755.

53. Christopher M, Eckfeldt J, Eaton J. Propylene glycol ingestion causes D-lactic acidosis. Laboratory investigation; a journal of technical methods and pathology. 1990;62(1):114-8.

54. Bowman CE, Rodriguez S, Alpergin ESS, Acoba MG, Zhao L, Hartung T, Claypool SM, Watkins PA, Wolfgang MJ. The mammalian malonyl-CoA synthetase ACSF3 is required for mitochondrial protein malonylation and metabolic efficiency. Cell Chemical Biology. 2017.

55. Hart DW, Wolf SE, Zhang X-J, Chinkes DL, Buffalo MC, Matin SI, DebRoy MA, Wolfe RR, Herndon DN. Efficacy of a high-carbohydrate diet in catabolic illness. Critical care medicine. 2001;29(7):1318-24.

56. Rousseau A-F, Losser M-R, Ichai C, Berger MM. ESPEN endorsed recommendations: nutritional therapy in major burns. Clinical nutrition. 2013;32(4):497-502.

57. Gore DC, Wolf SE, Sanford A, Herndon DN, Wolfe RR. Influence of metformin on glucose intolerance and muscle catabolism following severe burn injury. Annals of surgery. 2005;241(2):334.

58. Herndon DN, Hart DW, Wolf SE, Chinkes DL, Wolfe RR. Reversal of catabolism by beta-blockade after severe burns. New England Journal of Medicine. 2001;345(17):1223-9.

59. Flores O, Stockton K, Roberts JA, Muller MJ, Paratz JD. The efficacy and safety of adrenergic blockade after burn injury: A systematic review and meta-analysis. Journal of Trauma and Acute Care Surgery. 2016;80(1):146-55.

APPENDIX

```
##FactoMineR PCA package
install.packages(c("FactoMineR", "factoextra"))
library('FactoMineR')
library('factoextra')
burn=read.csv('BurnSerum time point.csv', check.names=FALSE)
log.burn=cbind(burn[,c(1,2)],log10(burn[,3:40]+0.0001))
log.burn.pca=PCA(log.burn[,c(-1,-2)],graph=FALSE)
#blue accent 1: 5B9BD5
#green accent 6: 70AD47
#grey-50% accent 3: A5A5A5
#orange accent 2: ED7D31
log.burn.scores=fviz_pca_ind(log.burn.pca,geom.ind='point',col.ind=burn$Timepoint,pal
ette='jco',addEllipses=TRUE ,mean.point=FALSE,xlab='PC1 (30.8%)',ylab='PC2
(20.8%)',legend.title='Time point')
#scree plot
log.burn.eig.viz=fviz_eig(log.burn.pca,addlabels=TRUE,ylim=c(0,50))
#contributions
log.burn.var.contrib.bar=fviz_contrib(log.burn.pca,choice='var',axes=1:2,top=38)
#biplot
log.burn.biplot=fviz_pca_biplot(log.burn.pca,col.ind=log.burn$Timepoint,palette='jco',ad
dEllipses=TRUE,mean.point=FALSE,label='var',col.var='black',select.var=list(name=c('
Acetoacetate','Isovalerate','X3.Hydroxybutyrate','X2.Hydroxybutyrate')),repel=TRUE,leg
end.title='Time point')
```

Supplemental Figure 1. R code for PCA of metabolite data with time point group information and confidence intervals. ‘Scores’ shows individual sample points plotted using the first two principal component scores for each sample. ‘Scree plot’ shows eigenvalues for each principal component. ‘Contributions’ shows contributions of individual metabolites to variability captured in a two-component PCA model. ‘Biplot’ adds contribution (loadings) vectors to the original scores plot.

Metabolite	0h mean	0h std. err.	24h mean	24h std. err.	48h mean	48h std. err.	72h mean	72h std. err.
2-Hydroxybutyrate	0.007	<0.001	0.011	<0.001	0.014	0.001	0.017	0.001
3-Hydroxybutyrate	0.002	<0.001	0.002	<0.001	0.005	<0.001	0.004	<0.001
Acetate	0.012	<0.001	0.006	<0.001	0.004	<0.001	0.004	<0.001
Acetoacetate	0.001	<0.001	0.002	<0.001	0.002	<0.001	0.003	<0.001
Acetone	0.001	<0.001	0.004	0.001	0.009	0.001	0.012	0.002
Alanine	0.033	0.001	0.039	0.001	0.022	<0.001	0.017	0.001
Betaine	0.022	<0.001	0.016	0.001	0.005	<0.001	0.002	<0.001
Carnitine	0.001	<0.001	0.002	<0.001	0.002	<0.001	0.001	<0.001
Choline	0.001	<0.001	0.001	<0.001	0.001	<0.001	0.001	<0.001
Creatine	0.013	0.001	0.076	0.003	0.066	0.005	0.034	0.002
Creatine phosphate	0.003	<0.001	0.005	<0.001	0.005	0.001	0.004	<0.001
Creatinine	0.007	<0.001	0.010	<0.001	0.010	0.001	0.005	<0.001
Glucose	0.349	0.006	0.335	0.007	0.327	0.011	0.257	0.013
Glutamate	0.012	<0.001	0.011	<0.001	0.010	0.001	0.008	<0.001
Glutamine	0.019	0.001	0.017	0.001	0.013	0.001	0.008	<0.001
Glycine	0.070	0.001	0.039	0.001	0.022	0.001	0.018	0.002
Histamine	0.006	<0.001	0.010	<0.001	0.008	0.001	0.005	<0.001
Hypoxanthine	0.002	<0.001	0.002	<0.001	0.003	<0.001	0.002	<0.001
Isobutyrate	0.001	<0.001	0.001	<0.001	0.001	<0.001	0.001	<0.001
Isoleucine	0.007	<0.001	0.012	<0.001	0.014	0.001	0.018	0.001
Isovalerate	0.001	<0.001	0.002	<0.001	0.003	<0.001	0.003	<0.001
Lactate	0.229	0.005	0.142	0.005	0.094	0.006	0.070	0.002
Leucine	0.011	<0.001	0.016	<0.001	0.011	<0.001	0.010	0.001
Lysine	0.005	<0.001	0.009	<0.001	0.010	<0.001	0.009	0.001
Malonate	0.006	<0.001	0.007	<0.001	0.003	<0.001	0.002	<0.001
Mannose	0.003	<0.001	0.005	<0.001	0.005	<0.001	0.005	<0.001
Methionine	0.003	<0.001	0.004	<0.001	0.002	<0.001	0.002	<0.001
N-Acetylglucosamine	0.001	<0.001	0.002	<0.001	0.004	<0.001	0.004	0.001
O-Phosphocholine	0.001	<0.001	0.001	<0.001	<0.001	<0.001	<0.001	<0.001
Phenylalanine	0.009	<0.001	0.017	<0.001	0.017	0.001	0.015	0.002
Proline	0.008	<0.001	0.010	<0.001	0.006	<0.001	0.005	0.001
Propylene glycol	0.003	<0.001	0.005	<0.001	0.009	0.001	0.013	0.002
Pyruvate	0.010	<0.001	0.008	<0.001	0.005	<0.001	0.004	<0.001
Succinate	0.001	<0.001	0.001	<0.001	<0.001	<0.001	0.001	<0.001
Threonine	0.009	<0.001	0.011	<0.001	0.010	<0.001	0.007	0.001
Trimethylamine-N-oxide	0.002	<0.001	0.003	<0.001	0.003	<0.001	0.002	<0.001
Tyrosine	0.005	<0.001	0.010	<0.001	0.007	<0.001	0.007	0.001
Valine	0.018	<0.001	0.030	0.001	0.025	0.001	0.029	0.003

Supplemental Table 1. Mean concentrations (mM) and standard errors of the means (mM) for individual metabolites at each time point. Raw values were not adjusted for dilution or filtration.